Enhanced Squeezing in Homodyne Detection via Local-Oscillator Optimization

by

Asif Shakeel

Submitted to the Department of Electrical Engineering and Computer Science in partial fulfillment of the requirements for the degree of

Master of Science

at the

MASSACHUSETTS INSTITUTE OF TECHNOLOGY

September 1995

Author .....
Department of Electrical Engineering and Computer Science
June 29, 1995

Certified by .....
Jeffrey H. Shapiro
Professor of Electrical Engineering
Thesis Supervisor

Accepted by .....
Frederic R. Morgenthaler
Chairman, Committee on Graduate Students

Enhanced Squeezing in Homodyne Detection via Local-Oscillator Optimization

by

Asif Shakeel

Submitted to the Department of Electrical Engineering and Computer Science in partial fulfillment of the requirements for the degree of

Master of Science

Abstract

Balanced homodyne detection of nonclassical (squeezed state) light sources yields noise levels below the semiclassical shot-noise value. This thesis addresses the problem of local-oscillator optimization for such homodyne arrangements. A system-theoretic framework is developed to search for the local-oscillator that minimizes the variance of the charge associated with the homodyne current. It is shown that the optimal local-oscillator can be found by solving a Fredholm equation. Given a general scheme for signal generation, the said formalism constitutes a rigorous framework to determine the minimum achievable noise level and the local-oscillator that attains that squeezing. From among the traditional squeezed state generation methods, fiber FWM is chosen for detailed study, using both instantaneous and non-instantaneous interaction. The optimal local-oscillator for the instantaneous case turned out to be a very narrow pulse coinciding with the peak of the pump pulse, properly phase-compensated for maximum squeezing. In the non-instantaneous case, important behavioral characteristics at high nonlinear phase-shifts were determined, although exact results for the optimum local-oscillators were not obtained. The optimal noise performance and exact solutions to the Fredholm equation were, however, calculated for a spatial interaction model with Gaussian Kerr-interaction spatial response.

Thesis Supervisor: Jeffrey H. Shapiro
Title: Professor of Electrical Engineering

This thesis is dedicated to my parents,

my father, Shakeel Ahmed

and

my mother, Bilquis Ahmed

Acknowledgements

It is rare that one comes in proximity with the strength and kindness of personality, and a mind so incisive as that of Professor Shapiro. I offer my deepest gratitude to him for everything from nurturing my incipient curiosity for some of the most exciting academic themes I have embarked on, to the guidance and encouragement he has generously imparted to take me through some very turbulent moments of my career.

I have had the privilege to learn from him his zest to uncover the fundamental questions, and his gift to formulate precisely and articulate clearly the physical and mathematical aspects of his ideas. Implicit is his agility in carrying those ideas to a completion, the sense of energy and intellectual integrity with which he inspires, and the confidence he places in his students. This thesis is a tribute to him.

If there is another presence whom I could always count on for a supporting voice, it is Professor Gould's. He had greater faith in me than I had in myself at times.

As a friend and as a source of sincere, rational advice is Professor Dahleh to whom I am doubly indebted for his role as a teacher and as an informal advisor.

From my group, I can unreservedly say that Jeff Bounds was unparalleled in helping me emerge alive from some of the most hair-raising encounters with "MABLE", for reading through my nerve-wracking attempts at the thesis write-up, generally keen insights about things quantum (on several occasions), and for his mirth and friendship.

I would like to extend thanks to Reggie Brothers for his concern about my well-being and sanity, and Steve Patterson for scintillating conversations that cast deep suspicion on the commutator games we play.

Bobby Lai, Dicky Lee, Donald Greer and Franco Wong have all been a positive influence on my growth both through the exchange of ideas in group meetings and around the office. Emma Presler is thanked for trying to salvage the remains of my humanity.

Among my colleagues, Peter Dodds has been *as* enlightening both on and off the field. His fluency in applied mathematics is matched only by his passion for cricket (bouncers followed by yorkers!). Julio Castrillon is hereby thanked for his vigorous opinions on system-theory related issues that came up. Sean Warnick, Jorge Goncalves, Ganesh N. Ramaswamy, Ahmed Mitwalli, John Ofori, Pierre Jalkh, Fadi Karameh, Omar Baba, and countless others are among the friends and well-wishers who kept my spirits up all the while.

In the graduate office, I would like to thank Marylin Pierce for not only taking care of the administrative complexities, but being so flexible and forthcoming in every aspect of the graduate life. Of course, without Peggy Carney's fellowship for the spring term, this thesis would be stillborn, and I thank her profusely for that. Monica for her caring attitude, and Lisa Bella for her cordiality and humor. Barbara for her cheerfulness and cultural depth. Mary Ziegler's assistance in tracking research papers is appreciated.

Penultimately, my companions and fellow Pakistanis, I am proud of you. Special thanks to Jalal Khan for being there throughout my dizzy days and for helping me balance academics and fitness, and to Asad Naqvi for absolutely superb discussions regarding the tricky mathematical and physics related subtleties. In no particular order, Adnan Lawai, Khurram Afridi, Salal Khan, Adil Bashir, Irfan-ullah Chaudhary, Ijaz Hussein, Salman Akhtar, Wasiq Bukhari, Farhan Rana, and Mustafa K. Ahmed, to you I owe (in all senses of the word) more than I can verbally express! Also, Kanwal Ejaz is gratefully acknowledged for her fruit trifles, and Hijab Chaudhary for the frequent dinners.

Ultimately, I need only say that nothing would have been possible had it not been for the unending love and patience of my family: my parents Shakeel and Bilquis Ahmed, my sister Mariam Ahmed, my brother Zafar Shakeel, and everyone else in our family near and afar. Their prayers, timely word and above all, fostering in me the freedom to pursue only the most challenging, forged the bridge over which I crossed this river.

Table of Contents

List of Figures

Chapter 1

Introduction

Fiber-optic communication systems and optical precision measurement systems are now achieving sensitivities approaching the ultimate limits set by their laser light sources. Performance analyses for such systems usually rely on semiclassical photodetection models. Semiclassically, it is the shot-noise resulting from the random charge-carrier generation produced in a photodetector in response to deterministic classical-field illumination that sets the ultimate photodetection sensitivity limit [1]. However, it has long been known that photodetection noise is of quantum-mechanical origin, and that sensitivity significantly better than the shot-noise limit can be achieved with light beams in appropriate nonclassical states [1]. The most popular arrangement to date for demonstrating such improvements has been balanced homodyne detection of squeezed state light. Because this thesis will be concerned with optimizing systems of this class, we devote most of this introductory chapter to a quick review of the quantum theory of homodyne detection, and squeezed state generation via fiber four-wave mixing.

1.1 Balanced homodyne detection

In balanced homodyne detection (see fig. 1), a signal field is mixed with a strong local-oscillator field through a 50/50 beam splitter onto a pair of detectors. The difference of the photocurrents from these detectors comprises a scaled, baseband version of that part of the signal field which is co-polarized, spatially coherent and in phase with the local-oscillator field, plus a shot-noise term.

The semiclassical theory of homodyne detection assumes that the measurement noise is shot-noise generated in the photodetector. In the high-intensity local-oscillator limit, this noise is predominantly local-oscillator shot-noise, conditioned on knowing the signal

field, and it has white, Gaussian statistics. The quantum theory, however, offers a different explanation. Here, in the strong local-oscillator limit with unity quantum efficiency detectors, the observation noise is due to the signal beam quantum noise.

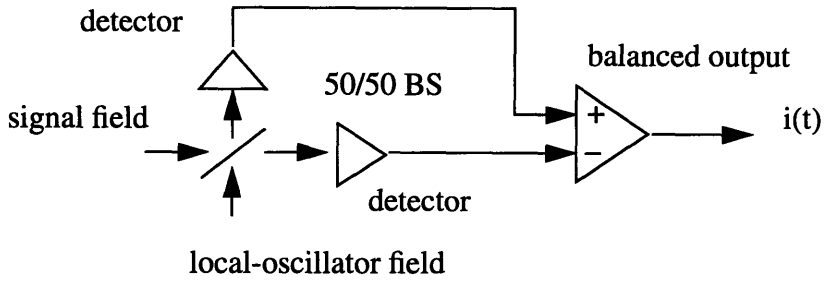

Fig. 1.1 Balanced homodyne detector

To be more explicit, let $E_S(t)$ and $E_{LO}(t)$ be the classical, photon-units, positive frequency fields entering the beam splitter in Fig. 1.1, where we have assumed spatially uniform beams and co-polarization, and we have suppressed the vectorial and spatial nature of the fields involved. Then, in the strong local-oscillator limit with unity quantum efficiency detectors, the output current satisfies [1]-[3]:

$$i(t) = 2qRe\left[E_S(t)\,E_{LO}^*(t)\right] + i_{shot}(t) \tag{1.1}$$

where q is the electron charge and $i_{shot}(t)$ is a zero-mean white Gaussian noise with covariance:

$$K_{i_{shot}\,i_{shot}}(t,u) = q^2\left|E_{LO}(t)\right|^2\delta(t-u) \tag{1.2}$$

Eqns. (1.1) and (1.2) are the semiclassical model for balanced homodyne detection. For the usual case of a continuous-wave local-oscillator, i.e., $E_{LO}(t) = \sqrt{P_{LO}}$, with P_{LO} being the photon flux, eq. (1.2) reduces to a stationary noise with spectral density q^2P_{LO}. This shot-noise level is the sensitivity limit of the semiclassical theory.

For the quantum treatment of balanced homodyne detection, the classical fields $E_S(t)$ and $E_{LO}(t)$ are replaced by quantum field operators, $\hat{E}_S(t)$ and $\hat{E}_{LO}(t)$, and the strong local-oscillator condition becomes placing $\hat{E}_{LO}(t)$ in a coherent state $|E_{LO}(t)\rangle$ of high photon flux. The resulting photocurrent, $i(t)$, turns out to have the same statistics as the quantum measurement:

$$\hat{i}(t) = 2qRe\left[\hat{E}_S(t)\,E_{LO}^*(t)\right] \tag{1.3}$$

If $\hat{E}_S(t)$ is in a coherent state $|E_S(t)\rangle$ then the mean function and covariance function of $\hat{i}(t)$ obey:

$$\langle\hat{i}(t)\rangle = 2qRe\left[E_S(t)\,E_{LO}^*(t)\right] \tag{1.4}$$

and

$$K_{\hat{i}\hat{i}}(t,u) = q^2\left|E_{LO}(t)\right|^2\delta(t-u) \tag{1.5}$$

reproducing the semiclassical results. However, there are quantum states which have lower homodyne-measurement noise than eq. (1.5) predicts, i.e., with states other than coherent states we can improve the sensitivity of a homodyne detector.

1.2 Squeezed states

Recently, there has been a great interest in the generation of squeezed states of the electromagnetic field. These are nonclassical light states with phase-sensitive noise that can lead to sub-shot-noise performance in optical homodyne detection [4]-[12].

In the fig.1 context, we can illustrate the potential of squeezed-state light by supposing that

$$\hat{E}_S(t) = \mu\hat{E}_{IN}(t) + \vartheta\hat{E}_{IN}^{\dagger}(t) \tag{1.6}$$

where μ, ϑ are real obeying $\mu^2 - \vartheta^2 = 1$, and $\hat{E}_{IN}(t)$ is in the vacuum state. We will

also assume that the local-oscillator is in the coherent state $|\sqrt{P_{LO}}e^{i\phi}\rangle$. Eqs. (1.3) and (1.6) then imply that:

$$\hat{i}(t) = 2q\sqrt{P_{LO}}Re\left[\left(\mu\hat{E}_{IN}(t) + \vartheta\hat{E}^{\dagger}_{IN}(t)\right)e^{-i\phi}\right] \tag{1.7}$$

which leads to:

$$K_{\hat{i}\hat{i}}(t,u) = q^2P_{LO}|\mu + \vartheta e^{-2i\phi}|^2\delta(t-u) \tag{1.8}$$

Eq. (1.8) is a phase-sensitive white-noise, whose normalized spectrum $|\mu + \vartheta e^{-2i\phi}|^2$ is plotted in Fig. 1.2 vs. ϕ, with $\mu = 2$, $\vartheta = \sqrt{3}$.

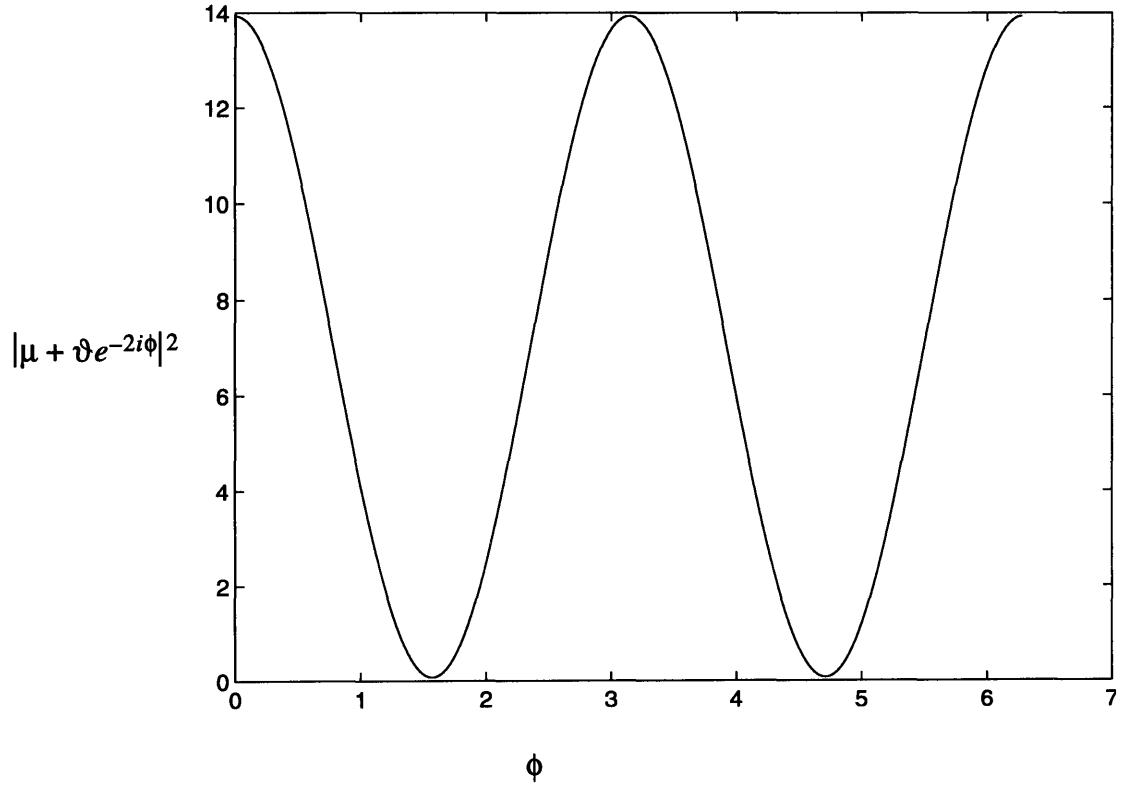

Fig. 1.2 Normalized current spectrum vs. local-oscillator phase

Note that the minimum value of this noise level is below the shot-noise (coherent state) level of q^2P_{LO} (1 in the normalized spectrum of Fig. 1.2). Because this noise arises from phase-sensitive "squeezing" of a vacuum-state $\hat{E}_{IN}(t)$, we say that $\hat{E}_S(t)$ is in a

squeezed vacuum state. It turns out that there are several nonlinear techniques which realize transformations like that given in eq. (1.6), among them are parametric amplification in $\chi^{(2)}$ nonlinear materials [5]-[7], and four-wave mixing (FWM) in $\chi^{(3)}$ nonlinear materials [8]-[11]. Of particular interest in this thesis is FWM in optical fiber.

1.3 Fiber Four-Wave Mixing

A simple, instantaneous-interaction model for squeezed-state generation in single-mode optical fiber is as follows (see Fig. 1.3)

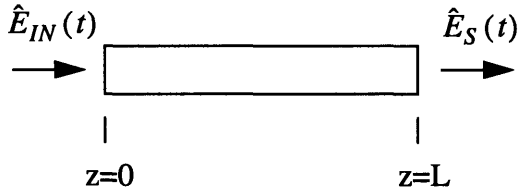

Fig. 1.3 Fiber input-output relation

Suppressing the transverse spatial characteristics of the fiber mode, we begin with the interaction occurring during propagation through L meters of fiber. In a frame of reference moving at the group velocity, v_g, of the center frequency, the spatio-temporal evolution of the single-mode field operator in the fiber is governed by:

$$\frac{\partial \hat{E}(z,t)}{\partial z} = i\kappa \hat{E}^{\dagger}(z,t)\,\hat{E}(z,t)\,\hat{E}(z,t) \tag{1.9}$$

where κ is the nonlinear phase-shift per unit photon flux, found from the physical dimensions of the fiber and the Kerr coefficient n_2 via:

$$\kappa = \frac{2\pi n_2 \hbar\omega}{A\lambda} \tag{1.10}$$

where $\hbar\omega$ is the photon energy at the laser frequency ω, λ is the wavelength at that frequency, and A is the fiber cross-sectional area.

Eq. (1.9) can be seen to have an analytical solution if one observes that the photon number operator, or classically the field intensity, is a constant of motion. The full self-phase modulation solution for the output operator in terms of the input operator is therefore:

$$\hat{E}_S(t) = \exp\Big(i\kappa L \hat{E}_{IN}^{\dagger}(t)\,\hat{E}_{IN}(t) \Big)\hat{E}_{IN}(t) \tag{1.11}$$

With a strong pump beam injected into the medium, a linearization in the powers of input fluctuation operators is possible, any terms higher than the first order in fluctuations being neglected, leading to:

$$\Delta\hat{E}_S(t) = \exp\Big(i\kappa L\left|E_{IN}(t)\right|^2 \Big)\Big[\Big(1 + i\kappa L\left|E_{IN}(t)\right|^2 \Big)\Delta\hat{E}_{IN}(t) + i\kappa L E_{IN}(t)^2 \Delta\hat{E}_{IN}^{\dagger}(t)\Big] \tag{1.12}$$

where $\Delta\hat{E}(t) = \hat{E}(t) - \langle\hat{E}(t)\rangle$ for the fiber input and output fields. This represents a Bogoliubov transformation of the type shown in eq. (1.6), i.e., it is commutator preserving and satisfies:

$$\begin{aligned} \Delta\hat{E}_S(t) &= \mu(t)\,\Delta\hat{E}_{IN}(t) + \vartheta(t)\,\Delta\hat{E}_{IN}^{\dagger}(t) \\ |\mu(t)|^2 - |\vartheta(t)|^2 &= 1 \end{aligned} \tag{1.13}$$

Experiments to observe the effect described here have been conducted by several researchers [5]-[7], [14]. Shirasaki and Haus [14] proposed a ring interferometer in which a Gaussian pulse is split by a 50/50 coupler and propagated in opposite directions around a fiber loop (see Fig. 1.4). Vacuum fluctuations enter through the unexcited port of the coupler and after mixing with the pulse within the loop, come out as squeezed vacuum from the same port. The phase modulated pump emerges from the other port and is used after augmenting it with a phase-shift $e^{i\phi}$, as the local-oscillator for homodyne detection of the squeezed vacuum.

We assign a peak amplitude $\sqrt{I_{IN}}$ and a pulse width τ_p to the pump pulse,

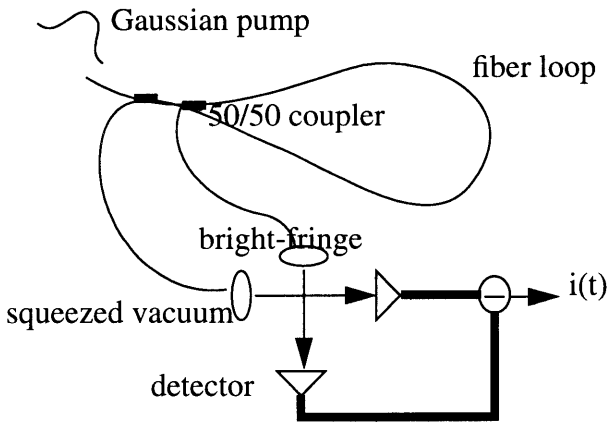

Fig. 1.4 Ring interferometer

$$E_{IN}(t) = \sqrt{I_{IN}}\exp\left(-\left(\frac{t}{\tau_p}\right)^2\right) \tag{1.14}$$

which undergoes a phase change through the nonlinear interaction before being used as the local-oscillator:

$$E_{LO}(t) = \exp\left(i\kappa L\left|E_{IN}(t)\right|^2\right)E_{IN}(t)\,e^{i\phi} \tag{1.15}$$

making the current covariance

$$K_{\hat{i}\hat{i}}(t,u) = q^2\left\{\begin{array}{c}\left|E_{LO}(t)\right|^2 + 2\kappa^2L^2\left|E_{LO}(t)\right|^2\left|E_{IN}(t)\right|^4 \\ + Re\left\{i2\kappa LE^{*2}{}_{LO}(t)\,E^2{}_{IN}(t)\,\left[1 + i\kappa L\left|E_{IN}(t)\right|^2\right]e^{-2i\phi}\right\}\end{array}\right\}\delta(t-u) \tag{1.16}$$

Unlike the simpler squeezed state of eq. (1.6), that gave rise to stationary white-noise statistics for the current, eq. (1.16) represents a non-stationary white-noise process. Here, a different noise measure than spectral density is needed, and the one defined by Joneckis and Shapiro [13] is the photoelectric charge variance. The operator measure for charge is:

$$\hat{q} = \int \hat{i}(t)\,dt \tag{1.17}$$

which has the variance:

$$\sigma^2_{\hat{q}} = var\left(\int \hat{i}(t)\,dt\right) = \int dt \int du K_{\hat{i}\hat{i}}(t,u) \tag{1.18}$$

Substituting eq. (1.16) into (1.18), the charge variance for fiber loop experiment becomes:

$$\sigma^2_{\hat{q}} = q^2\left\{\begin{array}{c}\int dt|E_{LO}(t)|^2 + 2\kappa^2 L^2 \int dt|E_{LO}(t)|^2|E_{IN}(t)|^4 \\ +2\kappa LRe\left(i\int dt E^{*2}{}_{LO}(t)\,E^2{}_{IN}(t)\,[1+i\kappa L|E_{IN}(t)|^2]\,e^{-2i\phi}\right)\end{array}\right\} \tag{1.19}$$

and can be minimized with respect to ϕ, to give:

$$\sigma^2_{\hat{q}_{min}} = q^2\left\{\begin{array}{c}\int dt|E_{LO}(t)|^2 + 2\kappa^2 L^2 \int dt|E_{LO}(t)|^2|E_{IN}(t)|^4 \\ -2\kappa L\left|\int dt E^{*2}{}_{LO}(t)\,E^2{}_{IN}(t)\,[1+i\kappa L|E_{IN}(t)|^2]\right|\end{array}\right\} \tag{1.20}$$

Our task is made easier because of the Gaussian pump and local-oscillator assumed. The analytical expression for eq. (1.20) follows:

$$\sigma^2_{\hat{q}_{min}} = q^2\left\{\begin{array}{c}\frac{\tau_p\sqrt{\pi}}{\sqrt{2}} + 2\kappa^2 L^2 I^2{}_{IN}\frac{\tau_p\sqrt{\pi}}{\sqrt{6}} \\ -2\kappa L I_{IN}\left|\frac{\tau_p\sqrt{\pi}}{2} + i\kappa L I_{IN}\frac{\tau_p\sqrt{\pi}}{\sqrt{6}}\right|\end{array}\right\} \tag{1.21}$$

Note that the product $\Phi_{NL} = \kappa L I_{IN}$ appears in the noise. This is the classical nonlinear phase-shift, due to fiber interaction, seen by the peak pump intensity. Eq. (1.21) can be written in terms of Φ_{NL}, and expanded in an asymptotic series for $\Phi_{NL} \gg 1$ to yield:

$$\sigma^2_{\hat{q}_{min}} = \frac{q^2\tau_p\sqrt{\pi}}{\sqrt{2}}\left\{1 - \frac{\sqrt{3}}{2} + \frac{3\sqrt{3}}{16\Phi^2{}_{NL}} + \text{-------}\right\} \tag{1.22}$$

from which it is apparent that at high Φ_{NL} the charge variance finds a lower limit. Gaussian pumps of higher peak intensity or longer fibers will not help decrease this floor further.

Had the signal field $\hat{E}_S(t)$ been in a coherent state, the charge variance would have been:

$$\sigma^2_{\hat{q}_{shot}} = \frac{q^2\tau_p\sqrt{\pi}}{\sqrt{2}} \tag{1.23}$$

Once again, this is going to be called shot-noise limit, and as a means of comparison, will be used to normalize eq. (1.22). The normalized charge-variance is therefore a dimensionless quantity with 1 representing the shot-noise level.

$$\sigma^2{}_N = \frac{\sigma^2_{\hat{q}_{min}}}{\sigma^2_{\hat{q}_{shot}}} = 1 - \frac{\sqrt{3}}{2} + \frac{3\sqrt{3}}{16\Phi^2{}_{NL}} + \text{- - - - - - -} \tag{1.24}$$

We now introduce the standard adopted for noise calculations, the squeezing factor (in decibels):

$$s_{min} = 10.\log_{10}[\sigma^2{}_N] \tag{1.25}$$

which has a minimum of -8.73 dB for the Haus-Shirasaki local-oscillator, and a shot-noise level of 0 dB. Compared to the calculated prediction, experimentally observed squeezing for $\chi^{(3)}$ fiber from Bergman and Haus [7] is about -5 dB. The discrepancy between the observed and the predicted noise reduction was attributed to stimulated Brillouin scattering.

The presence of noise-floor naturally leads us to the question regarding the existence of a local-oscillator that can perform better than the Haus-Shirasaki bright-fringe local-oscillator. There are two considerations here. The first is the criterion for optimality of a local-oscillator. The second is the particular local-oscillator that meets the criterion.

We can settle the first consideration as we did for the Haus-Shirasaki configuration: we normalize the charge variance for any local-oscillator and signal field state by its

value for the same local-oscillator and a coherent state field, i.e., by the shot-noise level for that local-oscillator. This, we know, is:

$$\sigma^2_{\hat{q}_{Shot}} = q^2 \int dt |E_{LO}(t)|^2 \tag{1.26}$$

With this normalization eq. (1.20) yields:

$$\sigma^2_N = \frac{\sigma^2_{\hat{q}_{min}}}{\sigma^2_{\hat{q}_{shot}}} = 1 + 2\kappa^2 L^2 \int dt |\xi_{LO}(t)|^2 |E_{IN}(t)|^4 - 2\kappa L \left| \int dt \xi_{LO}^{*2}(t) E^2_{IN}(t) \left[1 + i\kappa L |E_{IN}(t)|^2\right] \right| \tag{1.27}$$

The optimal local-oscillator is the $\xi_{LO}(t)$ that minimizes σ^2_N subject to the constraint:

$$\int dt |\xi_{LO}(t)|^2 = 1 \tag{1.28}$$

The second consideration can be addressed too. Eq. (1.27) points to the desired local-oscillator. Clearly σ^2_N is minimized if, at each time instant, the phase of $\xi_{LO}(t)$ is chosen to make:

$$\xi_{LO}^{*2}(t) E^2_{IN}(t) \left[1 + i\kappa L |E_{IN}(t)|^2\right] = |\xi_{LO}(t)|^2 |E_{IN}(t)|^2 \sqrt{1 + \kappa^2 L^2 |E_{IN}(t)|^4} \tag{1.29}$$

Defining a normalized pump field via:

$$e_{IN}(t) = \frac{E_{IN}(t)}{\sqrt{I_{IN}}} \tag{1.30}$$

eq. with the phase optimized $\xi_{LO}(t)$ becomes:

$$\sigma^2_N = \int dt |\xi_{LO}(t)|^2 \left[\sqrt{1 + \Phi^2_{NL} |e_{IN}(t)|^4} - \Phi_{NL} |e_{IN}(t)|^2\right]^2 \tag{1.31}$$

Because the term in square brackets is non-negative, and monotonically decreasing with increasing $\Phi_{NL} |e_{IN}(t)|^2$, and because $|\xi_{LO}(t)|^2$ is non-negative and integrates to 1, it is

obvious that the optimum $|\xi_{LO}(t)|^2$ must vanish at all times when $|e_{IN}(t)|^2 < max_t|e_{IN}(t)|^2 = 1$. For the Gaussian pump pulse in eq. (1.14), this means $|\xi_{LO}(t)|^2$ should be a unit-area impulse at t=0, in which case:

$$\sigma^2{}_N = \left[\sqrt{1+\Phi^2{}_{NL}} - \Phi_{NL}\right]^2 \quad . \tag{1.32}$$

Physically, the preceding optimization can be understood as follows. Eqs. (1.12) and (1.13) tell us that the signal fluctuations are a Bogoliubov transformation in the input fluctuations at any time t, and completely independent of the input fluctuations at all times other than t. If we were to choose a local-oscillator that was a very narrow pulse at time t_o such that $\mu(t)$ and $\vartheta(t)$ of eq. (1.13) (with direct counterparts in eq.(1.12)) stayed constant over the pulse duration, then the normalized charge variance as a function of t_o (minimized over the phase-shift) would be:

$$\sigma^2{}_N(t_o) = \left[\sqrt{1+\Phi^2{}_{NL}|e_{IN}(t_o)|^4} - \Phi_{NL}|e_{IN}(t_o)|^2\right]^2 \tag{1.33}$$

The normalized variance, which is the $|\xi_{LO}(t)|^2$-weighted integral of eq. (1.33), can be made no smaller in value than the lowest variance that can be obtained by varying t_o in eq. (1.33). The optimal local-oscillator is therefore a narrowly peaked pulse at the time of maximum signal squeezing.

The maximum squeezing occurs at the peak of the pump pulse, and is:

$$\sigma^2{}_N = \left[\sqrt{1+\Phi^2{}_{NL}} - \Phi_{NL}\right]^2 \tag{1.34}$$

It has an asymptotic expansion which goes down as $\frac{1}{4\Phi^2{}_{NL}}$ and has no noise-floor. Note that this is the same noise variance as the current spectrum one would get if one chose to drive the fiber with a continuous wave pump. The fluctuation operator in terms of Φ_{NL} is then:

$$\Delta\hat{E}_S(t) = \exp(i\Phi_{NL})\left[(1+i\Phi_{NL})\Delta\hat{E}_{IN}(t) + i\Phi_{NL}\Delta\hat{E}_{IN}{}^{\dagger}(t)\right] \tag{1.35}$$

which makes the minimum-noise current spectrum (see eq. (1.8)):

$$\left[\sqrt{1+\Phi^2_{NL}}-\Phi_{NL}\right]^2 \tag{1.36}$$

exactly the same as eq. (1.34). Thus, the best a local-oscillator can do in the instantaneous interaction case is to perform as well as the CW operation.

Although the preceding analyses are simple and appealing, they rely on an instantaneous interaction model which is known to be suspect. Indeed, certain experimentally observed and classically predicted effects are ruled out in the instantaneous interaction quantum picture. For example, Joneckis and Shapiro [17] have established that there is no self-phase modulation spectral broadening in instantaneous interaction quantum theory. Yet such self-phase modulation spectral broadening has long been observed. Joneckis and Shapiro go on to show that a finite response time (non-instantaneous) model can reconcile the observed effects with the theory. The finite response time turns out to be necessary even when the bandwidth of the input pulse does not approach the reciprocal interaction time of the nonlinearity. When the interaction between the fiber nonlinearity and the electromagnetic field is non-instantaneous, different frequencies in the pump input interact differently with the nonlinearity even in the FWM approximation, and the simple local-oscillator optimization procedure we developed above is no longer valid.

General formalism and specific fiber FWM results for local-oscillator optimization in squeezed state observations comprise the topics for this thesis. The remainder of the thesis is organized as follows.

1.4 Preview

In chapter 2 we build a general local-oscillator optimization framework presuming known second-order signal field statistics.

In chapter 3 we take a particular generation scheme -- fiber FWM -- and present a recently proposed model by Haus, Boivin and Kärtner [15] for continuous-time fiber inter-

action. We also choose a specific fiber response and relate it to the Raman noise model along the lines of Shapiro and Boivin [16].

In chapter 4 we use this model to look at a simple CW excitation of the fiber, and state the optimal LO for it. We make a comparison between the instantaneous interaction with the non-instantaneous interaction, identifying a new noise-floor in homodyne detection occurring at high nonlinear phase-shifts. We also trace the origins to the Raman noise in the fiber (cf. Shapiro-Boivin [16]).

In chapter 5 we generalize the results of chapter 4 to pulsed interactions, and show that there is an ultimate floor on squeezing that is determined by the fiber response, the pump, and the choice of local-oscillator. This is a significant result which sets a limit on FWM squeezing. In addition we translate some of the constraints imposed by the model to make a statement about a class of responses. We also illustrate our results for typical pump pulse excitations.

Chapter 6 alters the course of the thesis towards a slight generalization of the time-dependent FWM being studied. We demonstrate the predictive ability of the chapter 2 optimization framework by applying it to a spatial dependence in the FWM interaction. Clear analytical results are obtained for the optimal local-oscillator and a discussion is conducted of the squeezing improvement by comparing the performance of the optimal spatial local-oscillator mode with that of the suboptimal modes.

In chapter 7 we conclude the thesis by putting the results in a perspective, and indicate directions for future work.

Chapter 2

General Local-Oscillator Optimization Framework

The crux of the discussion at the conclusion of chapter 1 was the elegant solution to the problem of local-oscillator optimization for instantaneous interaction fiber FWM. A highly peaked (short pulse) local-oscillator timed to coincide with the peak of the pump pulse minimized the normalized charge variance at any Φ_{NL}, and obviated the noise-floor at high Φ_{NL}. Essential to the derivation of these results was the fact that the signal fluctuation operator at the output of the fiber was an instantaneous Bogoliubov transformation of the input fluctuation operator. Thus, the homodyne photocurrent covariance was a non-stationary white-noise for which local-oscillator optimization was straightforward. The purpose of this chapter is to establish a general framework for local-oscillator optimization, within which cases which do not generate non-stationary white-noise can be handled.

Rather than limit our attention to fiber FWM experiments, we shall consider balanced homodyne detection of an arbitrary signal field, whose second-order statistics are known, and seek a procedure for determining the normalized local-oscillator field $\xi_{LO}(t)$ that minimizes the normalized charge variance σ_N^2. In general, signal fields which are squeezed (i.e., which have $\sigma_N^2 < 1$) are produced by nonlinear optical interactions. Such interactions typically have a finite response time (unlike the instantaneous interaction we assumed in chapter 1) [15],[16], and may involve other noise degradations such as Brillouin scattering [7], dispersion and loss [18], or non-uniform nonlinear gains [20]. In circumstances like these, particular generation models dictate the specific signal covariances, and the search for an optimal local-oscillator is a non-trivial problem.

To keep the discussion simple, but general enough to highlight the key issues, we divorce ourselves from spatial variations in the field quantities, and assume that a generation-scheme analysis is available that provides second-order statistics for $\hat{E}_S(t)$, the sig-

nal field input to the homodyne detector. This generation scheme may be fiber FWM, parametric amplification, or some other system.

2.1 Normalized charge variance for general signal statistics

The normalized charge variance can be found from the current covariance via eq. (1.18) and the normalization condition eq. (1.26), with the following result:

$$\sigma^2{}_N = \frac{\int dt \int du K_{\hat{i}\hat{i}}(t,u)}{q^2 \int dt |E_{LO}(t)|^2} \tag{2.1}$$

The current covariance as defined through eq. (1.3) is:

$$K_{\hat{i}\hat{i}}(t,u) = \langle \hat{i}(t)\,\hat{i}(u) \rangle = 4q^2 \langle Re\left[\Delta\hat{E}_S(t)\,E_{LO}{}^*(t)\right] Re\left[\Delta\hat{E}_S(u)\,E_{LO}{}^*(u)\right] \rangle \tag{2.2}$$

Eq. (2.2) can be rewritten as:

$$\begin{aligned} K_{\hat{i}\hat{i}}(t,u) &= q^2 \langle \Delta\hat{E}_S(t)\,\Delta\hat{E}_S(u) \rangle E_{LO}{}^*(t)\,E_{LO}{}^*(u) \\ &+ q^2 \langle \Delta\hat{E}_S(t)\,\Delta\hat{E}_S{}^\dagger(u) \rangle E_{LO}{}^*(t)\,E_{LO}(u) \\ &+ q^2 \langle \Delta\hat{E}_S{}^\dagger(t)\,\Delta\hat{E}_S(u) \rangle E_{LO}(t)\,E_{LO}{}^*(u) \\ &+ q^2 \langle \Delta\hat{E}_S{}^\dagger(t)\,\Delta\hat{E}_S{}^\dagger(u) \rangle E_{LO}(t)\,E_{LO}(u) \end{aligned} \tag{2.3}$$

Several observations about the terms in eq. (2.3) permit some simplification. The second term can be reduced through the commutation relation for free-field operators:

$$[\Delta\hat{E}_S(t), \Delta\hat{E}_S(u)] = 0 \tag{2.4}$$

$$\left[\Delta\hat{E}_S(t), \Delta\hat{E}_S{}^\dagger(u)\right] = \delta(t-u) \tag{2.5}$$

to:

$$q^2\langle\Delta\hat{E}_S(t)\,\Delta\hat{E}_S^{\dagger}(u)\rangle E_{LO}^{*}(t)\,E_{LO}(u) = E_{LO}^{*}(t)\,E_{LO}(u)\,\delta(t-u) + \langle\Delta\hat{E}_S^{\dagger}(t)\,\Delta\hat{E}_S(u)\rangle^{*}E_{LO}^{*}(t)\,E_{LO}(u) \tag{2.6}$$

where we have also used the fact that the normally-ordered covariance $\langle\Delta\hat{E}_S^{\dagger}(t)\,\Delta\hat{E}_S(u)\rangle$ is Hermitian. Next, because the phase-sensitive covariance $\langle\Delta\hat{E}_S(t)\,\Delta\hat{E}_S(u)\rangle$ is symmetric in t, u, the first and the fourth terms are complex conjugates. Eq. (2.3) now reduces to:

$$K_{\hat{i}\hat{i}}(t,u) = q^2\left|E_{LO}(t)\right|^2\delta(t-u) + 2q^2Re\{\langle\Delta\hat{E}_S(t)\,\Delta\hat{E}_S(u)\rangle E_{LO}^{*}(t)\,E_{LO}^{*}(u)\} + 2q^2Re\{\langle\Delta\hat{E}_S^{\dagger}(t)\,\Delta\hat{E}_S(u)\rangle E_{LO}(t)\,E_{LO}^{*}(u)\} \tag{2.7}$$

It is expedient at this point to introduce a simpler notation for the phase-sensitive and the normally-ordered covariances:

$$K^{(p)}(t,u) = \langle\Delta\hat{E}_S(t)\,\Delta\hat{E}_S(u)\rangle \qquad K^{(n)}(t,u) = \langle\Delta\hat{E}_S^{\dagger}(t)\,\Delta\hat{E}_S(u)\rangle \tag{2.8}$$

and write the normalized charge variance from eq. (2.1) with the use of eq. (2.7) as:

$$\sigma^2{}_N = 1 + 2\int dt\int du K^{(n)}(t,u)\,\xi_{LO}(t)\,\xi_{LO}^{*}(u) + 2Re\int dt\int du K^{(p)}(t,u)\,\xi_{LO}^{*}(t)\,\xi_{LO}^{*}(u) \tag{2.9}$$

where we have used the property that the normally-ordered covariance is a positive semi-definite Hermitian function of t, u, and $\xi_{LO}(t)$ is the normalized local-oscillator field as introduced in chapter 1.

2.2 Framework construction and optimal local-oscillator description

It is not very obvious from eq. (1.8) what the optimal local-oscillator should be. There is a transformation, however, that makes clear how one might determine the optimal local-

oscillator. Suppose the covariances are expanded in terms of their real and imaginary parts:

$$K^{(p)}(t,u) = K_R{}^{(p)}(t,u) + iK_I{}^{(p)}(t,u) \tag{2.10}$$

$$K^{(n)}(t,u) = K_R{}^{(n)}(t,u) + iK_I{}^{(n)}(t,u) \tag{2.11}$$

and that the local-oscillator is mapped to a 2-D vector comprising its real and imaginary parts:

$$\gamma(t) = \begin{bmatrix} Re\{\xi_{LO}(t)\} \\ Im\{\xi_{LO}(t)\} \end{bmatrix} \tag{2.12}$$

Then the normalized charge variance acquires an inner product structure:

$$\sigma^2{}_N = 1 + 2\int dt \int du \gamma(t)^T K(t,u)\gamma(u) \tag{2.13}$$

where:

$$K(t,u) = \left[\begin{array}{c|c} K_R{}^{(p)}(t,u) + K_R{}^{(n)}(t,u) & K_I{}^{(n)}(t,u) + K_I{}^{(p)}(t,u) \\ \hline K_I{}^{(p)}(t,u) - K_I{}^{(n)}(t,u) & K_R{}^{(n)}(t,u) - K_R{}^{(p)}(t,u) \end{array}\right] \tag{2.14}$$

The matrix $K(t,u)$ is a symmetric real-valued matrix function of t, u, because of the symmetry properties of $K^{(p)}(t,u)$, $K^{(n)}(t,u)$. Thus it has orthonormal vector eigenfunctions and real eigenvalues satisfying:

$$\int du K(t,u)\Phi_i(u) = \lambda_i \Phi_i(t) \tag{2.15}$$

$$\int dt \Phi_i(t)^T \Phi_j(t) = \delta_{ij} \tag{2.16}$$

Because $\sigma_N^2 \geq 0$, we have that: $\lambda_i \geq -\frac{1}{2}$; the optimum local-oscillator $\xi_{LO}(t)$ in its com-

ponent form is:

$$\begin{bmatrix} Re\{\xi_{LO}(t)\} \\ Im\{\xi_{LO}(t)\} \end{bmatrix} = \Phi_{min}(t) \tag{2.17}$$

where $\Phi_{min}(t)$ is the solution to (2.15), (2.16) with minimum associated eigenvalue λ_{min}; and:

$$\sigma^2_N = 1 + 2\lambda_{min} \tag{2.18}$$

is the optimum normalized charge variance achieved with this local-oscillator choice.

2.3 Approaches to find the optimal local-oscillator

On a purely computational level, we might ask if we have made a headway by posing the problem in a new guise. At the very least, a clear separation of the problem has been achieved. Any optical system can be imagined to function as the signal generation scheme, and regardless of how complicated a normally-ordered and phase-sensitive covariance it produces, we know for certain that there exists a local-oscillator to minimize the charge variance.

We will quickly overview the possible courses we can adopt to go on from here, and present in a condensed form some of the techniques that exist for problems like these. If we are content with a purely numeric result to our optimization problem, standard techniques like discretization in time followed by computation of eigenvectors using matrix methods can be used. That certainly is a path which will let us numerically compute the optimal local-oscillator [21] for any generation scheme. Also, since we do not really need to know the eigenvalues other than the minimum, it might be best to specialize and reach for variational techniques that allow that eigenvalue and associated eigenvector to be com-

puted. There is a body of literature [21], [22], that deals specifically with such issues, and certain robust algorithms exist for computations like these.

Moreover, the existence of an orthonormal basis of eigenvectors also creates a useful opportunity to choose instead of a discrete time approach, an approach that uses a finite basis of orthonormal vectors chosen intelligently to be as close to the actual basis as can be guessed, and then the kernel matrix can be projected onto the basis to get a finite order matrix whose eigenvalues and eigenvectors are computed [21]. In all of the numerical methods, the trade-off between accuracy and computational prowess has to be balanced.

These observations are handy if a numerical solution is our eventual aim. Our goal, however, is to gain some insight from the matrix formalism. As we go through the rest of the thesis, we will allude to our framework in this chapter to address and support some of the findings we present.

Chapter 3

The Non-instantaneous Interaction Model for Fiber FWM

As mentioned in chapter 1, this thesis specializes its optimum local-oscillator development to squeezed state generation via fiber FWM. In this chapter we introduce a non-instantaneous interaction model for fiber FWM. Among the various efforts [17], [23], [24] to find a model for non-instantaneous interaction in optical fiber, the model by Boivin, Kärtner, and Haus [23], is probably the best. It is a continuous time treatment that properly preserves commutator brackets and includes the necessary Raman noise source. The Boivin, Kärtner, and Haus model addresses the full self-phase modulation case. In later work, Shapiro and Boivin [16] specialized this model to CW fiber FWM. We build on the Shapiro and Boivin model by generalizing it slightly to include pulsed FWM. Note that only the n_2 interaction is modeled: group velocity dispersion and loss are ignored, i.e., they are assumed to be negligible.

3.1 The Haus-Boivin-Kärtner model in FWM regime

In the notation of chapter 1, the signal field fluctuation operators are related to the input fluctuation operators and the strong pump pulse by:

$$\Delta\hat{E}_S(t) = e^{\left[iL\int h(t-\tau)\left|E_{IN}(\tau)\right|^2 d\tau\right]}\begin{pmatrix} i\hat{\Theta}(t)\,E_{IN}(t) + \Delta\hat{E}_{IN}(t) \\ + iL\int h(t-\tau)\,E_{IN}{}^{*}(\tau)\,\Delta\hat{E}_{IN}(\tau)\,E_{IN}(t)\,d\tau \\ + iL\int h(t-\tau)\,E_{IN}(\tau)\,\Delta\hat{E}_{IN}{}^{\dagger}(\tau)\,E_{IN}(t)\,d\tau \end{pmatrix} \tag{3.1}$$

where $h(t)$ is the real-valued, causal, non-instantaneous impulse response of the Kerr effect in the fiber. For comparison, the instantaneous interaction model would have

$h(t) = \kappa\delta(t)$. In the non-instantaneous interaction model we have $\kappa = H(0)$, where

$$H(\omega) = \int dt\,[h(t)\,e^{i\omega t}] \tag{3.2}$$

is the frequency response associated with $h(t)$.

In eq. (3.1) $\hat{\Theta}(t)$ is an Hermitian noise operator that commutes with $\Delta\hat{E}_{IN}(t)$, $\Delta\hat{E}_{IN}^{\dagger}(t)$, and has zero-mean Gaussian statistics with symmetrized correlation:

$$\langle\hat{\Theta}(t)\,\hat{\Theta}(u) + \hat{\Theta}(u)\,\hat{\Theta}(t)\rangle = \frac{L}{\pi}\int H_i(\omega)\coth(\hbar\omega/2kT)\cos[\omega(t-u)]\,d\omega \tag{3.3}$$

where $H_i(\omega) = Im\{H(\omega)\}$. Physically, $\hat{\Theta}(t)$ originates from molecular vibrations in the fiber, thus it represents the noise due to Raman scattering. As we can see from eq. (3.3), not only does the noise depend on the imaginary part of the nonlinear index of the material, i.e., the energy conversion between the electromagnetic field and the medium, it also has a temperature dependence through the $\coth(\hbar\omega/2kT)$ term. At higher temperatures this term has a greater contribution at each frequency, and is indicative of heightened molecular vibrations. The overall effect of the noise source is to mask the signal noise at all frequencies and temperatures, and hence reduce squeezing.

The Raman noise operator has the following commutator:

$$[\hat{\Theta}(t), \hat{\Theta}(u)] = -i\frac{L}{\pi}\int H_i(\omega)\sin[\omega(t-u)] \tag{3.4}$$

This commutator preserves the commutators of the field operators as they propagate through the medium. In order to ensure a self-consistent theory, the only additional requirement we must impose is that $H_i(\omega)$ be non-negative for $\omega > 0$.

3.1.1 Relation of the Raman Gain to $H_i(\omega)$

$H_i(\omega)$ is closely related to the Raman gain [25],[26] of the medium, as it determines the rate of growth of the signal fluctuations because of the conversion of pump photons to

signal photons through interactions with the medium. The exact relation between the low frequency Raman gain and $H_i(\omega)$ as derived by Shapiro and Boivin [16] is:

$$\frac{2H_i(\Delta\omega)A}{\hbar\omega_p} = G_o\left(a(\Delta\omega) + b(\Delta\omega)^3\right) \tag{3.5}$$

where various parameters in eq. (3.5) can be found in ref. [16].

At this point it is relevant to note that certain stringent limits are placed in choosing a model for the fiber response $h(t)$. These arise from the requirements $H_i(\omega) \geq 0$ for $\omega > 0$ in conjunction with $\langle \hat{\Theta}^2(t) \rangle < \infty$ Both $H_i(\omega)$ and $\coth(\hbar\omega/2kT)$ are odd functions and both remain positive for positive frequencies with $\coth(\hbar\omega/2kT)$ asymptotically going to 1 as $\omega \to \infty$. Thus, applying $\langle \hat{\Theta}^2(t) \rangle < \infty$ in eq. (3.2) we see that $H_i(\omega)$ must be absolutely integrable. In other words, for a proper model we have to choose a causal real-valued $h(t)$ whose fourier transform has an imaginary part that obeys:

$$H_i(\omega) \geq 0 \text{ for } \omega > 0, \qquad \int \frac{d\omega}{2\pi} |H_i(\omega)| < \infty \tag{3.6}$$

There still is some freedom in the model because the exact form of the response function is not given, only some conditions it has to meet. Next we deploy a response, originally used by Boivin-Haus-Kärtner, that matches the real fiber parameters for response time and self-phase modulation coefficient and justify that it meets all the requirements laid down so far.

3.2 Two-pole fiber response

Experimentally, it is known that the fiber response takes time delays on the order of 1-100fs. The CW response has a Kerr coefficient given by κ, which therefore equals $H(0)$. Also, the link between the Raman gain and $H_i(\omega)$ puts strict condition on the slope of

$H_i(\omega)$ at ω=0. We need to have enough parameters in the response to satisfy the criteria just mentioned. The simplest one that does so is a two-pole response of the form:

$$h(t) = \kappa \frac{\Omega^2}{\sqrt{\Omega^2 - \Gamma^2/4}} e^{-\frac{\Gamma}{2}t} \sin\left[\left(\sqrt{\Omega^2 - \Gamma^2/4}\right)t\right] u(t) \tag{3.7}$$

$$H(\omega) = \frac{\kappa\Omega^2\left(\Omega^2 - \omega^2\right) + i\kappa\Omega^2\omega\Gamma}{\left(\Omega^2 - \omega^2\right)^2 + \omega^2\Gamma^2} \tag{3.8}$$

Assuming a response time of 1 fs, we have $\Gamma = 2.10^{15}\ s^{-1}$, and using the values of physical parameters like the mode area A of $2.33 \times 10^{-11}\ m^2$, pump wavelength ω_p corresponding to 795 nm wavelength, and the slope of $H_i(\omega)$ at ω=0 from Shapiro-Boivin calculations [16]:

$$H_i'(0) = 2.05 \times 10^{-36}\ s^2/m \tag{3.9}$$

we have:

$\kappa = 2.71 \times 10^{-21}$ s/m, and the resonance parameter $\Omega = 1.626 \times 10^{-15}\ s^{-1}$.

We can see from eq. (3.8) that $H_i(\omega)$ is positive for positive frequencies and goes down as $\frac{1}{\omega^3}$ for $\omega \gg 1$ which means that it is absolutely integrable.

3.3 Verification of the FWM approximation

Since we cannot be sure *apriori* that FWM is a valid approximation to work with, we should be careful to stay within the range of pump powers and fiber lengths that characterize experiments involving squeezing of pulses. We are interested in applying our local-oscillator optimization to experiments like Bergman and Haus [7], which typically have fiber loops 25 meters long and peak pump intensities of Watts.

The main disparity between quantum self-phase modulation and quantum FWM is the decay of the mean-field amplitude as the pulse propagates through the fiber. We need to establish what constitutes a strong pump regime, i.e., minimal mean-field decay, and here a certain degree of arbitrariness can be exercised. To keep a conservative outlook, any mean-field decay of greater than 1 dB will be considered prohibitive to FWM. To understand the decay, one looks at the full SPM mean field result [16]:

$$\langle \hat{E}_S(t) \rangle = e^{-\langle \hat{\Theta}^2(0) \rangle} e^{\int d\tau \, [\exp[iLh(t-\tau)] - 1] \left| E_{in}(\tau) \right|^2} E_{IN}(t) \tag{3.10}$$

The noise term contributes to the decay, and implies that for a dB of decay, one requires a fiber length of:

$$\frac{0.1}{\log(e)} \left[\frac{1}{2\pi} \int H_i(\omega) \coth(\hbar\omega/2kT) d\omega \right]^{-1} \tag{3.11}$$

where we have assumed that the term:

$$e^{\int d\tau \, [\exp[iLh(t-\tau)] - 1] \left| E_{in}(\tau) \right|^2} \tag{3.12}$$

has a negligible decay at the lengths concerned. Typically the decay length from eq. (3.11) is around 30 km for the two-pole response, with T=0 K. Expression (3.12) is on the order of $e^{-10^{-10}}$ for this fiber length and a 1 ps pump pulse of peak intensity 1 Watt, confirming our guess that it causes comparatively insignificant decay. At higher temperatures the 1 dB decay length shrinks, but stays well above the experimentally accessible range. Since the mean-field decay has no dependence on the pump intensity and increases at higher fiber lengths, higher phase-shifts Φ_{NL} are best achieved by shorter fibers and higher pump intensities.

Now that we have constructed a response which is physically relevant, and know that our approximation is valid in the regime of interest -- 25 meters long fiber and peak pump intensities on the order of Watts, the noise computations can be begun.

Chapter 4

Continuous Wave Local-Oscillator Optimization

The simplest pump that can be used to drive a nonlinear medium is a CW pump, and this, as we saw in chapter 1, has a white-noise spectrum for an instantaneous fiber interaction. For a non-instantaneous interaction, there is a simple extension to the instantaneous case, with the twist that now the fluctuations have both a linear transformation through the fiber response and a thermal noise exacerbating the phase noise.

4.1 Non-instantaneous interaction with CW excitation

In the linearized regime of FWM, eq. (3.1) with a coherent state CW pump of average amplitude $\sqrt{I_{IN}}$ becomes:

$$\Delta\hat{E}_S(t) = e^{i\kappa LI_{IN}} \begin{pmatrix} i\hat{\Theta}(t)\sqrt{I_{IN}} + \Delta\hat{E}_{IN}(t) \\ + iLI_{IN}\int h(t-\tau)\,\Delta\hat{E}_{IN}(\tau)\,d\tau \\ + iLI_{IN}\int h(t-\tau)\,\Delta\hat{E}_{IN}^{\dagger}(\tau)\,d\tau \end{pmatrix} \tag{4.1}$$

This represents a linear time-invariant transformation from $\Delta\hat{E}_{IN}(t), \Delta\hat{E}_{IN}^{\dagger}(t)$ to $\Delta\hat{E}_S(t), \Delta\hat{E}_S^{\dagger}(t)$ and an added noise term. Because the inputs (including the additive noise) have stationary statistics, so will the outputs. We naturally select the frequency domain as the domain of choice to carry out optimization, because there the signal fluctuations are uncorrelated between different frequencies. We cast aside the pure phase term, $e^{i\kappa LI_{IN}}$, in eq. (4.1), as it can be made a part of the local-oscillator phase $e^{i\phi}$. Fourier transforming the fluctuation operator, we get:

$$\hat{E}_S(\omega) = \begin{matrix} i\sqrt{I_{in}}\hat{\Theta}(\omega) + [1 + iLI_{IN}H(\omega)]\,\Delta\hat{E}_{IN}(\omega) \\ + iLI_{IN}H(\omega)\,\Delta\hat{E}_{IN}^{\dagger}(-\omega) \end{matrix} \tag{4.2}$$

4.2 Frequency domain representation of noise

Just as in eq. (1.24), spectral calculations are best done in terms of a peak nonlinear phase-shift:

$$\Phi_{NL} = \kappa L I_{IN} \tag{4.3}$$

which requires us to normalize the fiber response to:

$$\begin{aligned} h(t) &= \kappa g(t) \\ H(\omega) &= \kappa G(\omega) = \kappa [G_r(\omega) + iG_i(\omega)] \end{aligned} \tag{4.4}$$

The normally-ordered and the phase-sensitive spectra defined as:

$$\begin{aligned} S^{(n)}(\omega) &= \int d\tau K^{(n)}(t+\tau, t)\, e^{i\omega\tau} \\ S^{(p)}(\omega) &= \int d\tau K^{(p)}(t+\tau, t)\, e^{i\omega\tau} \end{aligned} \tag{4.5}$$

turn out to be the following:

$$S^{(n)}(\omega) = \Phi_{NL}(G_i(\omega)\coth(\hbar\omega/2kT) + G_i(\omega)) + \Phi_{NL}^2|G(\omega)|^2 \tag{4.6}$$

$$S^{(p)}(\omega) = \Phi_{NL}(-G_i(\omega)\coth(\hbar\omega/2kT) + iG_r(\omega)) - \Phi_{NL}^2|G(\omega)|^2 \tag{4.7}$$

The signal has a center frequency of $\omega = 0$ and homodyning assumes a local-oscillator at the same center frequency as the signal field. We, therefore, choose a CW local-oscillator as follows:

$$E_{LO}(t) = \sqrt{P_{LO}}e^{i\phi} \tag{4.8}$$

and optimize ϕ at the ω we want to observe. We then measure the noise at the phase-optimized ω and get:

$$S_N(\omega) = 1 + 2Ev\left[S^{(n)}(\omega)\right] - 2\left|S^{(p)}(\omega)\right| \tag{4.9}$$

where Ev represents the even part of the spectrum.

Substituting eqs. (4.6) and (4.7) in eq. (4.9) we get:

$$S_N(\omega) = \frac{1 + 2\Phi_{NL}\left[G_i(\omega)\coth(\hbar\omega/2kT) + \Phi_{NL}|G(\omega)|^2\right]}{-2\Phi_{NL}\sqrt{\left[G_i(\omega)\coth(\hbar\omega/2kT) + \Phi_{NL}|G(\omega)|^2\right]^2 + G_r^2(\omega)}} \tag{4.10}$$

Ordinarily, the CW pump, CW local-oscillator case 'measures' $S_N(\omega)$ by using a spectrum analyzer on $i(t)$ and the minimum noise is obtainable by tuning over the analyzer frequency. However, the CW and pulsed analyses can be unified as follows: assume a CW pump, calculate $\sigma^2{}_N$ (the normalized charge variance) using:

$$\xi_{LO}(t) = \begin{cases} \sqrt{\frac{2}{T}}\cos(\omega t - \phi) & |t| \le \frac{T}{2} \\ 0 & \text{elsewhere} \end{cases} \tag{4.11}$$

with ϕ arbitrary and $T \to \infty$. ϕ optimization will yield the same normalized charge variance as the spectrum of eq. (4.10).

The subtle difference between the present CW pump, CW local-oscillator non-instantaneous case and the instantaneous response pulsed case is that here we are faced with a transformation which is not a Bogoliubov transformation, so the simple peak μ, ϑ arguments do not apply. The optimal frequency for a given Φ_{NL} depends on both the particular response function chosen and on the temperature of the fiber.

4.3 Noise spectrum for the two-pole response

Given the temperature T of the fiber, eq. (4.10) shows the effect that a general fiber response has on the noise at different frequencies. The Raman noise comes in through the term:

$$G_i(\omega)\coth(\hbar\omega/2kT) \tag{4.12}$$

which peaks near the peak of $G_i(\omega)$. Fig. 4.1 plots $G_i(\omega)$ and displays its peak at $\approx 10^{15}$ rad/s. The degree of squeezing depends on the relative magnitudes of $G_i(\omega)$ and

$G_r(\omega)$ with greater squeezing resulting at the frequencies which have higher $|G_r(\omega)|$ compared to $G_i(\omega)$. The explanation behind this observation is that higher $|G_r(\omega)|$ stand for a stronger Kerr-interaction and higher squeezing, whereas high $G_i(\omega)$ imparts more Raman noise.

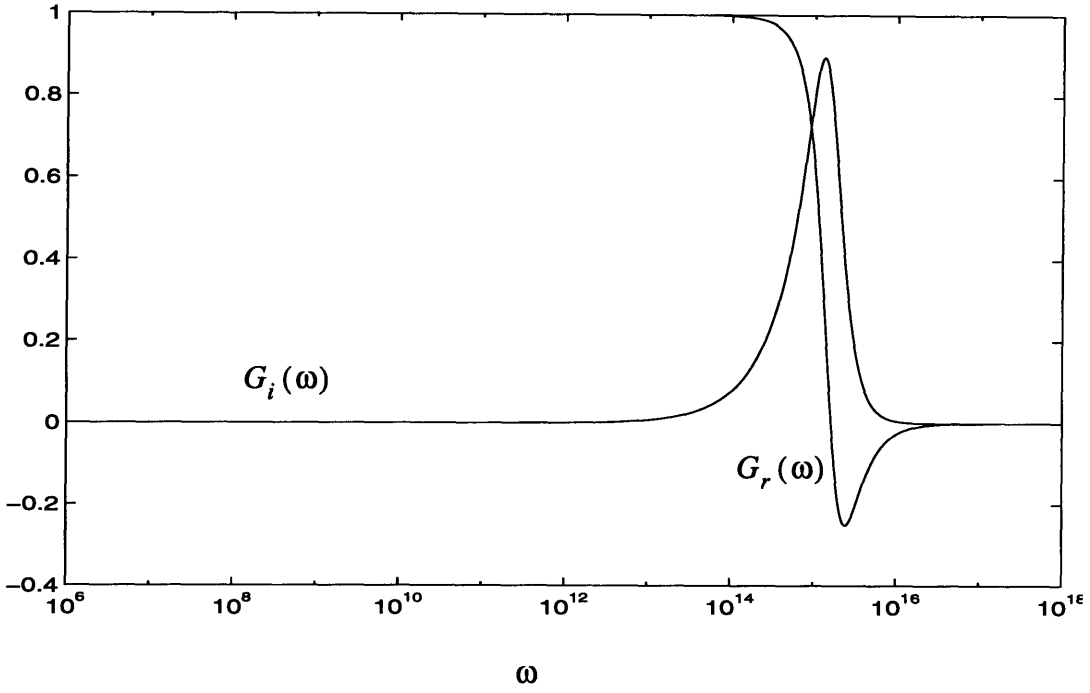

Fig. 4.1 A comparison of the real and imaginary parts of the Fourier transform of the normalized response function.

Fig. 4.2 shows $S_N(\omega)$ vs. ω for T=0 and T=300 K at $\Phi_{NL} = 1$. At a given temperature, squeezing is better at low frequencies with higher $|G_r(\omega)|$ and smaller $G_i(\omega)$. The spectrum reaches the shot-noise level, $S_N(\omega) = 1$, where $G_r(\omega) = 0$ and no Kerr-interaction exists. Also evident from Fig. 4.2 is the variation of squeezing with temperature, with squeezing getting worse at all frequencies as temperature rises.

The special case of $\omega = 0$ has been investigated by Shapiro and Boivin [16]. Because of the discontinuity in coth($\hbar\omega$/2kT) at $\omega = 0$, eq. (4.10) reconfigures to become:

$$S_N(0) = \begin{Bmatrix} 1 + 2\Phi_{NL}\left[\frac{2kT}{\hbar}G_i'(0) + \Phi_{NL}\right] \\ -\Phi_{NL}\sqrt{\left[\frac{2kT}{\hbar}G_i'(0) + \Phi_{NL}\right]^2 + 1} \end{Bmatrix} \tag{4.13}$$

There is an explicit temperature dependence here, and at T=0 the spectrum reduces to the instantaneous model of eq. (1.36). As a consequence, the leading term in the asymptotic expansion of $S_N(0)$ is $\frac{1}{4\Phi^2_{NL}}$, and $S_N(0)$ decreases monotonically at high Φ_{NL}. At non-zero temperatures, the leading term changes to $2kTG_i'(0)/\hbar\Phi_{NL}$ which is considerably higher than $\frac{1}{4\Phi^2_{NL}}$. This is a purely Raman induced noise, which has an ostensible presence at all frequencies, and its effect is to block the squeezing performance.

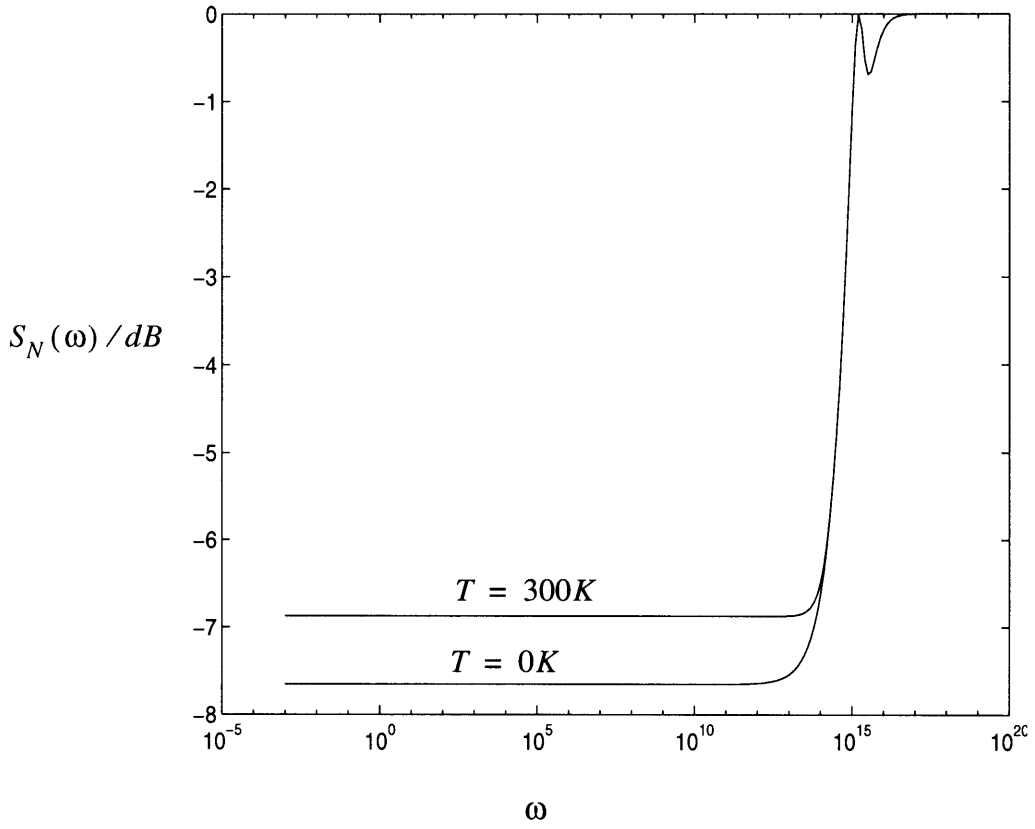

Fig. 4.2 CW spectrum vs. frequency for the two-pole response. Comparison of T=0 K and T=300 K spectra for $\Phi_{NL} = 1$ rad.

Apart from these remarks which depend on the exact frequency and temperature under study, we would like to find any ultimate limits imposed on the spectrum as higher Φ_{NL} are approached. We must first ascertain that this limit is not unrealistic. The peak pump intensity required to give us a Φ_{NL} of 1 rad is:

$$P_{IN} = \hbar\omega_P I_{IN} = \frac{\hbar\omega_P}{\kappa L} \tag{4.14}$$

For L=25 meters, we get $\Phi_{NL} = 1$ rad when $P_{IN} = 2.75$ Watts. Pulsed pumps can have peaks much higher than this, thus phase-shifts greater than 1 are achievable.

4.4 Asymptotic expansion of the noise spectrum

We continue the analysis in the vein of eq. (1.22), in the limit of $\Phi_{NL} \gg 1$, expanding eq. (4.10) in an asymptotic series:

$$S_N(\omega) = \left[\begin{array}{l} 1 - G_r^2(\omega)/|G(\omega)|^2 \\ +\dfrac{1}{\Phi_{NL}|G(\omega)|^2} G_i(\omega)\coth(\hbar\omega/2kT)x \\ \left(G_i^2(\omega)\coth^2(\hbar\omega/2kT) + G_r^2(\omega)\right) \\ +\dfrac{1}{4\Phi_{NL}^2|G(\omega)|^6}\left(G_i^2(\omega)\coth^2(\hbar\omega/2kT) + G_r^2(\omega)\right)x \\ \left[-5G_i^2(\omega)\coth^2(\hbar\omega/2kT) + G_r^2(\omega)\right] \\ \qquad\qquad + \text{- - - - - - - - - - - - -} \end{array}\right] \tag{4.15}$$

The noise pattern away from $\omega = 0$ is rather different from what Shapiro and Boivin [16] discussed. Now we come across a lowest achievable noise as $\Phi_{NL} \to \infty$ because it is no longer true that $G_r(\omega) = |G(\omega)| = 1$ at $\omega > 0$. The term independent of Φ_{NL} in eq. (4.15) represents that noise-floor and it equals the shot-noise level of 1 for those ω which have $G_r(\omega) = 0$. The next few terms in the expansion basically determine the rate at

which the floor is approached. In particular, higher temperatures mean a decelerated decline of the noise with Φ_{NL} and higher magnitudes of $G_i(\omega)$ have the same effect. On the other hand, a larger magnitude of $G_r(\omega)$ has the effect of making the floor lower through the term independent of Φ_{NL}, but simultaneously arresting the approach through the next term in $\frac{1}{\Phi_{NL}}$.

4.4.1 Noise-floor for the two-pole response

If we take the two-pole response as the fiber response model and plot the squeezing at some selected frequencies against Φ_{NL}, as in Fig. 4.3, the trends outlined above are visible. Close to the peak of $G_i(\omega)$, around $\omega = 1e15$ rad/s, $G_r(\omega)$ is very small in magnitude, and this amounts to both the noise-floor rising up through the ratio $G_r^2(\omega)/|G(\omega)|^2$ and the rate of decline of the noise with Φ_{NL} becoming slower because of the peaking of $G_i(\omega)$. The $\omega = 0$ plots show no flattening out except that the T= 300K plot slopes down much slower than the T=0 plot as the remarks following eq. (4.14) emphasize. The T=0 slope is ≈ -20 dB/decade in the log-log plot of Fig. 4.3, whereas the T=300K plot goes only as ≈ -10 dB/decade. The $\omega = 1e15$ rad/s plot, however, has a base. If we use the floor terms from eq. (4.15), it evaluates to -2.226 dB for the response we have, which is exactly as it appears in the plot. Since the relative magnitudes of $G_i(\omega)$ and $G_r(\omega)$ change appreciably only after $\omega = 1e14$ rad/s, the floor for frequencies lower than this is negligibly small and the squeezing essentially follows the $\omega = 0$ plot at least to the Φ_{NL} shown. As the electronically observable bandwidth is about 10 GHz, the noise-floor is a phenomenon undetectable in the CW case, two-pole response.

To recapitulate, we have made a quantitative analysis of the noise spectrum for CW case in this chapter. We have also obtained clean limits to the high Φ_{NL} squeezing and the factors that cause it to be retarded. These insights will reappear in a different form in the

next chapter where we generalize the results to a pulsed pump interaction and obtain limits of similar nature.

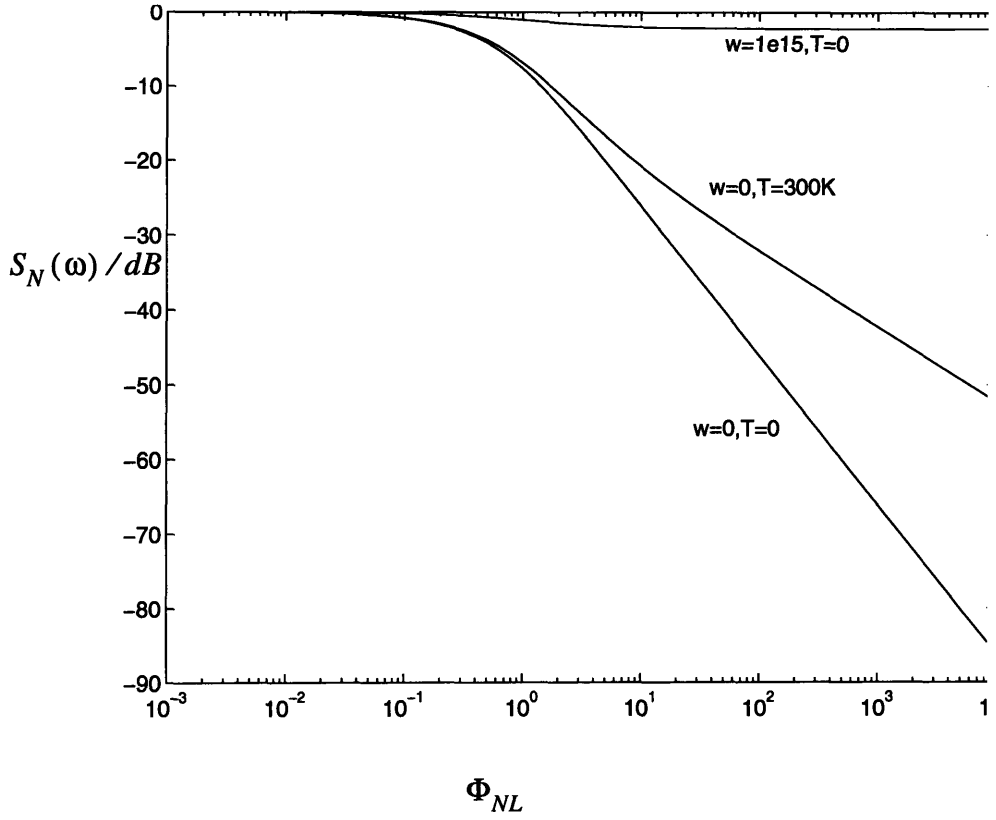

Fig. 4.3 Squeezing floor and decay vs. nonlinear phase-shift at different frequencies and temperatures

Chapter 5

Local-Oscillator Optimization for Non-Instantaneous Pulsed FWM

As a point of departure for the pulsed interaction, we may begin by elaborating on eq. (3.1) more thoroughly. We have not yet had a reason to attach any significance to the presence of the pump pulse inside the superposition integrals in this equation. It turns out that the pump pulse has a very profound influence on the noise behavior. For the CW case considered in chapter 4, the normally-ordered and phase-sensitive field covariances were stationary, because these were convolution integrals relating $\Delta\hat{E}_{IN}(t), \Delta\hat{E}_{IN}^{\dagger}(t)$ to $\Delta\hat{E}_{S}(t), \Delta\hat{E}_{S}^{\dagger}(t)$. With a pulsed pump, however, the input operators are multiplied by the pump pulse both before and after their being convolved with the fiber response. In the frequency domain this leads to a mixing of frequencies, which produces correlations between frequencies such that the output signal's covariance is no longer stationary either in time or in frequency.

We can easily derive the signal covariances of eq. (2.8) for the eq. (3.1) FWM model in terms of a general response $h(t)$ and an assumed state for the input fluctuations. Let us assume that the input fluctuations are in a vacuum state:

$$\begin{aligned} \langle \Delta\hat{E}_{IN}^{\dagger}(t)\, \Delta\hat{E}_{IN}(u) \rangle &= 0 \\ \langle \Delta\hat{E}_{IN}(t)\, \Delta\hat{E}_{IN}(u) \rangle &= 0 \end{aligned} \tag{5.1}$$

Then with the aid of eq. (3.1) and its Hermitian conjugate, we can readily compute the output signal covariances. Without the loss of generality we shall ignore the chirp modulation term in eq. (3.1), because during optimization it can be absorbed in the local-oscillator phase, as can be seen from eq. (2.2). The output signal covariances are:

$$K^{(n)}(t,u) = \begin{bmatrix} \frac{L}{2\pi}\int H_i(\omega)\coth(\hbar\omega/2kT)\cos[\omega(t-u)]\,d\omega \\ +\frac{i}{2}L[h(u-t)-h(t-u)] \\ +L^2\int h(t-\tau)\,h(u-\tau)\left|E_{IN}(\tau)\right|^2 d\tau \end{bmatrix} E_{IN}^*(t)\,E_{IN}(u) \tag{5.2}$$

$$K^{(p)}(t,u) = \begin{bmatrix} -\frac{L}{2\pi}\int H_i(\omega)\coth(\hbar\omega/2kT)\cos[\omega(t-u)]\,d\omega \\ +\frac{i}{2}L[h(u-t)+h(t-u)] \\ -L^2\int h(t-\tau)\,h(u-\tau)\left|E_{IN}(\tau)\right|^2 d\tau \end{bmatrix} E_{IN}(t)\,E_{IN}(u) \tag{5.3}$$

The rest of the thesis adheres to the assumption that the fluctuations are in a vacuum state, so eqs. (5.2) and (5.3) remain the basic covariance expressions.

The kernel matrix of eq. (2.14), in terms of the normalized functions and parameters, becomes:

$$K(t,u) = \left[\begin{array}{c|c} 0 & \Phi_{NL}g(u-t) \\ \hline \Phi_{NL}g(t-u) & \left(\begin{array}{c} \frac{\Phi_{NL}}{\pi}\int G_i(\omega)\coth(\hbar\omega/2kT)\cos[\omega(t-u)]\,d\omega \\ +2\Phi_{NL}{}^2\int g(t-\tau)\,g(u-\tau)\,e_{IN}^2(\tau)\,d\tau \end{array}\right] \end{array}\right] \text{x}$$

$$e_{IN}(t)\,e_{IN}(u) \tag{5.4}$$

In principle, we need only find the minimum-eigenvalue eigenfunction of eq. (2.16) with the kernel of eq. (5.4). However, as described below, we shall take a more circuitous, but more insightful route.

The earlier cases of instantaneous response (chapter 1) and the CW pump (chapter 4) were first analyzed for an optimal local-oscillator which then enabled statements about the noise at high nonlinear phase-shifts. Those were tight lower bounds on the achievable noise performance and there existed local-oscillators that actually met those bounds at all Φ_{NL}. Such statements are very tough to make for the kernel of eq. (5.4), because it does not admit to an obvious analytical form for the optimal local-oscillator, or even a non-trivial noise bound at all nonlinear phase-shifts. A viable strategy, which we shall take, is to search for a lower bound on σ_N^2, the normalized charge variance, and then look for local-oscillators which approach that bound. Implicit in this argument is the dependence of the bound on the response function and the pump profile.

Following our experience in the CW case, and given our interest in high Φ_{NL}, strong squeezing, we will make an asymptotic expansion of σ_N^2 and optimize its behavior by appropriate local-oscillator choice.

5.1 Asymptotic expansion at high nonlinear phase-shift

The investigation of this limit begins with eq. (2.9). First we assume that the local-oscillator has the form:

$$\xi_{LO}(t) = \rho_{LO}(t)\, e^{i\phi} \tag{5.5}$$

and choose the constant phase ϕ to make the phase-sensitive term in eq. (2.9) a negative real quantity. The phase optimized charge variance, ${\sigma_N}^2$, is then:

$$\begin{aligned} {\sigma^2}_N = \; & 1 + 2\int dt \int du K^{(n)}(t,u)\, \rho_{LO}(t)\, {\rho_{LO}}^*(u) \\ & -2\left|\int dt \int du K^{(p)}(t,u)\, \rho_{LO}{}^*(t)\, {\rho_{LO}}^*(u)\right| \end{aligned} \tag{5.6}$$

We can compute this charge variance for the Haus-Boivin model by substituting eqs. (5.2) and (5.3) in eq. (5.6):

$$\sigma_N^2 = 1 + 2\int dt \int du \left[\begin{array}{c} \frac{\Phi_{NL}}{2\pi}\int G_i(\omega)\coth(\hbar\omega/2kT)\cos[\omega(t-u)]\,d\omega \\ +\frac{i}{2}\Phi_{NL}[g(u-t)-g(t-u)] \\ +\Phi_{NL}^2\int g(t-\tau)\,g(u-\tau)\left|e_{IN}(\tau)\right|^2 d\tau \end{array} \right] \begin{array}{l} \text{x } e_{IN}^*(t)\,\rho_{LO}(t) \\ \text{x } e_{IN}(u)\,\rho_{LO}^*(u) \end{array}$$

$$-2\left| \int dt \int du \left[\begin{array}{c} -\frac{\Phi_{NL}}{2\pi}\int G_i(\omega)\coth(\hbar\omega/2kT)\cos[\omega(t-u)]\,d\omega \\ +\frac{i}{2}\Phi_{NL}[g(u-t)+g(t-u)] \\ -\Phi_{NL}^2\int g(t-\tau)\,g(u-\tau)\left|e_{IN}(\tau)\right|^2 d\tau \end{array} \right] \begin{array}{l} \text{x } e_{IN}(t)\,\rho_{LO}^*(t) \\ \text{x } e_{IN}(u)\,\rho_{LO}^*(u) \end{array} \right| \tag{5.7}$$

At high phase-shifts $\Phi_{NL} \gg 1$, so the dominating terms are those in Φ_{NL}^2. We single out the coefficients of Φ_{NL}^2 from the normally-ordered and the phase-sensitive terms above,

$$\begin{aligned} \sigma_N{}^2 &\approx \int dt \int du \psi(t)\,\psi^*(u) \int d\tau g(t-\tau)\,g(u-\tau)\left|e_{IN}(\tau)\right|^2 \\ &-\left| \int dt \int du \psi^*(t)\,\psi^*(u) \int d\tau g(t-\tau)\,g(u-\tau)\left|e_{IN}(\tau)\right|^2 \right| \end{aligned} \tag{5.8}$$

where: $\psi(t) = e_{IN}^*(t)\,\rho_{LO}(t)$

Next we assert:

$$\begin{aligned} &\int dt \int du \psi(t)\,\psi^*(u) \int d\tau g(t-\tau)\,g(u-\tau)\left|e_{IN}(\tau)\right|^2 \\ &\geq \left| \int dt \int du \psi^*(t)\,\psi^*(u) \int d\tau g(t-\tau)\,g(u-\tau)\left|e_{IN}(\tau)\right|^2 \right| \end{aligned} \tag{5.9}$$

Proof:

The normally-ordered coefficient (LHS) can be expressed as:

$$\begin{aligned}
&\int dt \int du \psi(t)\,\psi^*(u) \int d\tau g(t-\tau)\, g(u-\tau) \left|e_{IN}(\tau)\right|^2 \\
&= \int d\tau \left|e_{IN}(\tau)\right|^2 \left[\int g(t-\tau)\,\psi(t)\,dt\right]\left[\int g(u-\tau)\,\psi(u)\,du\right]^* \\
&= \int d\tau \left|e_{IN}(\tau)\right|^2 \left|\left[\int g(t-\tau)\,\psi(t)\,dt\right]\right|^2
\end{aligned} \tag{5.10}$$

Similarly, the phase-sensitive coefficient (RHS) can be written:

$$\begin{aligned}
&\int dt \int du \psi^*(t)\,\psi^*(u) \int d\tau g(t-\tau)\, g(u-\tau) \left|e_{IN}(\tau)\right|^2 \\
&= \int d\tau \left|e_{IN}(\tau)\right|^2 \left[\int g(t-\tau)\,\psi(t)\,dt\right]^{*2}
\end{aligned} \tag{5.11}$$

Applying the triangle inequality to eq. (5.11), the assertion becomes clear.

This result has a direct impact on the limit calculation. We can apply the triangle inequality to the phase-sensitive term in eq. (5.7) and state:

$$\begin{aligned}
&\left|\int dt \int du \left[\begin{array}{c} -\dfrac{\Phi_{NL}}{2\pi}\int G_i(w)\coth(\hbar\omega/2kT)\cos\left[\omega(t-u)\right]d\omega \\ +\dfrac{i}{2}\Phi_{NL}\left[g(u-t)+g(t-u)\right] \\ -\Phi_{NL}^2\int g(t-\tau)\,g(u-\tau)\left|e_{IN}(\tau)\right|^2 d\tau \end{array}\right]\psi^*(t)\,\psi^*(u)\right| \\
&\leq \left[\begin{array}{c} \Phi_{NL}^2\left|\int dt\int du\int d\tau g(t-\tau)\,g(u-\tau)\left|e_{IN}(\tau)\right|^2\psi^*(t)\,\psi^*(u)\right| \\ +\left|\int dt\int du\left[\begin{array}{c} -\dfrac{1}{2\pi}\int G_i(\omega)\coth(\hbar\omega/2kT)\cos\left[\omega(t-u)\right]d\omega \\ +\dfrac{i}{2}\left[g(u-t)+g(t-u)\right] \end{array}\right]\psi^*(t)\,\psi^*(u)\right| \end{array}\right]
\end{aligned} \tag{5.12}$$

and similarly the normally-ordered term is subject to:

$$\int dt \int du \begin{bmatrix} \frac{\Phi_{NL}}{2\pi} \int G_i(\omega) \coth(\hbar\omega/2kT) \cos[\omega(t-u)]\, d\omega \\ + \frac{i}{2}\Phi_{NL}[g(u-t) - g(t-u)] \\ + \Phi_{NL}^2 \int g(t-\tau)\, g(u-\tau) \left| e_{IN}(\tau) \right|^2 d\tau \end{bmatrix} \psi(t)\, \psi^*(u)$$

$$\geq \begin{bmatrix} \Phi_{NL}^2 \int dt \int du \int d\tau g(t-\tau)\, g(u-\tau) \left| e_{IN}(\tau) \right|^2 \psi^*(t)\, \psi(u) \\ - \Phi_{NL} \left| \int dt \int du \begin{bmatrix} \frac{1}{2\pi} \int G_i(\omega) \coth(\hbar\omega/2kT) \cos[\omega(t-u)]\, d\omega \\ + \frac{i}{2}[g(u-t) - g(t-u)] \end{bmatrix} \psi(t)\, \psi^*(u) \right| \end{bmatrix} \tag{5.13}$$

from which it follows that:

$$\sigma_N^2 \geq 1 + 2\Phi_{NL}^2 \left(\begin{array}{l} \int d\tau \left| e_{IN}(\tau) \right|^2 \left| \left[\int g(t-\tau)\, \psi(t)\, dt \right] \right|^2 \\ - \left| \int d\tau \left| e_{IN}(\tau) \right|^2 \left[\int g(t-\tau)\, \psi(t)\, dt \right]^{*2} \right| \end{array} \right) + O(\Phi_{NL}) \tag{5.14}$$

where $O(\Phi_{NL})$ terms are of order Φ_{NL} or lesser.

Eq. (5.14) shows the effect of a local-oscillator choice on the noise behavior at high Φ_{NL}. From eq. (5.9), the term in Φ_{NL}^2 is non-negative. If a fixed local-oscillator is chosen for which the coefficient of Φ_{NL}^2 is a positive quantity, then as Φ_{NL} grows, σ_N^2 eventually blows up because of this term. Therefore, the optimum local-oscillator must depend on the particular Φ_{NL}, and keep decreasing the coefficient of Φ_{NL}^2 with increasing Φ_{NL}. At higher and higher Φ_{NL}, this coefficient must go towards 0.

The convergence of the Φ_{NL}^2 coefficient to 0 does not imply that a local-oscillator that makes this term 0 is the optimal one at a given Φ_{NL}, because the other terms can still off-set this reduction in σ_N^2. The purpose of the argument above is to allow us to surmise the limits on σ_N^2 at high Φ_{NL} and possibly deduce a limiting form of the function towards which the local-oscillator tends as higher Φ_{NL} are approached.

There is one more observation we need before we can state an interesting result. From eq. (5.7) we see that we can replace the pump by a non-negative real function, because the only place where pump phase matters is in the product $\psi(t) = e_{IN}^*(t)\,\rho_{LO}(t)$. Therefore the pump phase can be completely absorbed in the local-oscillator phase. Without loss of generality, therefore, the pump term $e_{IN}(t)$ will be assumed to be real and non-negative.

Now we can show that at high nonlinear phase-shifts, with $e_{IN}(t) \geq 0$, the optimal local-oscillator, $\rho_{LO}(t)$, tends to a constant phase function.

The coefficient of Φ_{NL}^2 in eq. (5.14) is non-negative from eq. (5.9). It is zero if and only if $\psi(t)$ is real to within a constant phase (triangle inequality). If $\psi(t)$ has a given time-dependent phase, then the coefficient of Φ_{NL}^2 is non-zero in eq. (5.14) and Φ_{NL} can be made arbitrarily large to make the value of σ_N^2 be any positive number. This implies that as Φ_{NL} increases, the optimal local-oscillator must adjust its phase to become closer to having a constant phase.

Having established the above asymptotic condition on optimal local-oscillator, we shall assume a local-oscillator of the form: $\rho_{LO}(t) = \zeta(t)\,e^{i\theta}$, with $\zeta(t)$ real, and minimize σ_N^2 as a function of θ. We start with:

$$\sigma_N^2(\theta) = 1 + 2\left[A_1\Phi_{NL} + A_2^2\Phi_{NL}^2\right](1-\cos 2\theta) + 2B\Phi_{NL}\sin 2\theta \tag{5.15}$$

where:

$$A_1 = \int dt \int du \frac{1}{2\pi}\int d\omega G_i(\omega)\coth(\hbar\omega/2kT)\cos\left[\omega(t-u)\right] e_{IN}(t)\,e_{IN}(u)\,\zeta(t)\,\zeta(u) \tag{5.16}$$

$$A_2^2 = \int du\left(\int dt\zeta(t)\,g(t-u)\,e_{IN}(t)\right)^2 e_{IN}^2(u) \tag{5.17}$$

$$\begin{aligned} B &= \int du\int dt\zeta(t)\,e_{IN}(t)\,g(t-u)\,\zeta(u)\,e_{IN}(u) \\ &= \int du\int dt\zeta(t)\,e_{IN}(t)\,g_e(t-u)\,\zeta(u)\,e_{IN}(u) \end{aligned} \tag{5.18}$$

$g_e(t)$ being the even part of the response function.

We optimize over θ to get the lowest possible noise for a real $\zeta(t)$, and then expand in the powers of Φ_{NL} with the following result:

$$\sigma_N^2(\Phi_{NL}) = 1 - \frac{B^2}{A_2^2} + \frac{B^2 A_1}{A_2^4 \Phi_{NL}} + \frac{B^4 - 4B^2 A_1^2}{4A_2^6 \Phi_{NL}^2} + \text{- - - - - - - - - - -} \tag{5.19}$$

The noise-floor, a term chosen to describe:

$$lim_{\Phi_{NL} \to \infty} \sigma_N^2 \tag{5.20}$$

determined by the Φ_{NL} independent terms in the expansion, can be made zero if $\frac{B^2}{A_2^2} = 1$. By a method similar to the one employed before in proving eq. (5.9), it can be shown that $B^2 \le A_2^2$. $|B|$ can be written as:

$$\begin{aligned} |B| &= \left| \int du \int dt \zeta(t)\, e_{IN}(t)\, g(t-u)\, \zeta(u)\, e_{IN}(u) \right| \\ &\le \left(\int dt \zeta^2(t) \right)^{1/2} \left[\int du \left(\int dt \zeta(t)\, e_{IN}(t)\, g(t-u)\, e_{IN}(u) \right)^2 \right]^{1/2} \\ &= \left[\int du \left(\int dt \zeta(t)\, e_{IN}(t)\, g(t-u) \right)^2 e_{IN}^2(u) \right]^{1/2} = A_2 \end{aligned} \tag{5.21}$$

Equality holds if and only if

$$\int du e_{IN}(t)\, g(t-u)\, e_{IN}(u)\, \zeta(u) = \lambda \zeta(t) \tag{5.22}$$

for some non-zero λ and $\zeta(t)$.

We have come to another Fredholm equation. If a solution to eq. (5.22) can be found for a given pump $e_{IN}(t)$, and a response $g(t)$, then we know that at high phase-shifts, the noise-floor can be eliminated. Let us first check if this condition makes sense for the simple cases we have already analyzed. For an instantaneous response, eq. (5.22) becomes:

$$e_{IN}^2(t)\, \zeta(t) = \lambda \zeta(t) \tag{5.23}$$

which is the same as saying that a narrow pulse timed wherever $e_{IN}(t) \neq 0$ should get rid of the floor. This is indeed true if we look at eq. (1.33) which has no noise-floor at any t_o,

although the optimal local-oscillator must coincide with the peak pump intensity. We wonder if such a nice result exists for all $g(t)$.

The two-pole response is illustrative of what happens in those situations in which $g(t)$ arises from a finite number of poles and zeros and has no impulsive part in it, unlike the instantaneous response.

For the two-pole response, $g(t) = 0$ for $t \leq 0$. The kernel of the Fredholm equation in eq. (5.22) is then a strictly causal kernel or a Volterra kernel, i.e., $e_{IN}(t)\, g(t-u)\, e_{IN}(u)\, \zeta(u) = 0$ for $t \leq u$. Theorem 5.3.3.3 of ref. [27] states that for a strictly causal operator A, and for every non-zero λ, the operator $\lambda I - A$ is invertible. So no non-zero λ exists for which eq. (5.22) can be satisfied.

This does not in and of itself mean that the noise-floor is not removable, but it would be interesting to know if we run into a problem like this only for the two-pole response we chose or if there is a statement hidden in the constraints placed by eq. (3.6) on the response, that makes $g(0) = 0$ for some class of allowed responses. We already have that $g(t) = 0$ for $t < 0$ from the causality of $g(t)$.

As it turns out, the absolute integrability and phase requirements on $G_i(\omega)$ imposed by eq. (3.6) are quite binding on $g(t)$. For a real causal $g(t)$, the Fourier transform's real and imaginary parts are a Hilbert transform pair, and it can be shown that as long as the Laplace transform of the response is a rational function of two polynomials in the transform variable s, and satisfies eq. (3.6), there must be exactly two more poles than zeros of $G(s)$.

Proof:

Part 1: If $G(s) = \dfrac{Z(s)}{P(s)}$ is the Laplace transform of a real function $g(t)$,

$$G(s) = \int g(t)\, e^{st} dt \tag{5.24}$$

where $P(s) = s^p + a_{p-1}s^{p-1} + \text{-------} + a_0$, $Z(s) = s^z + b_{z-1}s^{z-1} + \text{-------} + b_0$, s.t.

$p \geq z+1$, and $G(\omega)$ has an absolutely integrable imaginary part, $G_i(\omega)$, then $p \geq z+2$.

Proof of part 1:

The assumption $p \geq z+1$ ensures that the response function has no impulses or its derivatives. $iG_i(\omega)$ is the Fourier transform of the odd part of the real function $g(t)$. The Laplace transform of the odd part is thus:

$$g_o(t) = \frac{1}{2}[g(t) - g(-t)] \leftrightarrow G_o(s) = \frac{1}{2}[G(s) - G(-s)] \tag{5.25}$$

where

$$G_i(\omega) = \frac{1}{i}G_o(i\omega) \tag{5.26}$$

which implies

$$G_o(s) = \frac{1}{2}\frac{[Z(s)P(-s) - Z(-s)P(s)]}{P(s)P(-s)} \tag{5.27}$$

The order of the numerator in eq. (5.24) is at most p+z and that of the denominator is 2p. If $G_i(\omega)$ is to be absolutely integrable, then it must decay at least as fast as $\frac{1}{\omega^2}$. This requires that the order of the denominator be at least two greater than that of the numerator. If $p \geq z+2$, integrability is assured. Assume this is not so, that is, p = z+1. Then the p+z power terms in the numerator of $G_o(s)$ must cancel to achieve the requisite condition. But this is impossible if p=z+1, from the form of $G_o(s)$: it requires $s^z(-s)^p - (-s)^z s^p = 2(-1)^{z+1}s^{2z+1} = 0$. Hence $p \geq z+2$ if $G_i(\omega)$ is to be absolutely integrable.

Part 2:

If $G_i(\omega)$ for a real, causal $g(t)$ satisfies:

$$G_i(\omega) \geq 0 \text{ for } \omega > 0, \qquad \int \frac{d\omega}{2\pi}|G_i(\omega)| < \infty \tag{5.28}$$

and $G(0) > 0$, then the number of poles must be exactly two greater than the number of

zeros in $G(s)$.

Proof:

For this, one needs to look at the frequency dependence of the phase of $G(\omega)$. The phase is given by

$$\arg[G(\omega)] = n\pi + \sum_i \arg(j\omega - z_i) - \sum_j \arg(j\omega - p_j) \tag{5.29}$$

where p_j and z_i are pole and zero locations on the s-plane respectively. The term $n\pi$ ensures that $G(0) > 0$. According to our convention for Laplace transform (see eq. (5.24)), the poles are in the right half-plane, since $g(t)$ represents a causal, stable response, and the zeros can be anywhere on the s-plane. All the poles and zeros must appear in complex conjugate pairs, or be on the real axis.

By eq. (5.28), the phase must also be bounded by $0 \leq \arg[G(\omega)] \leq \pi$. In the limit $\omega \to \infty$, the poles change the phase from their $\omega = 0$ values by a total of $p\frac{\pi}{2}$ and zeros, at the most, by phase of $-\frac{z\pi}{2}$. If $p \geq z + 3$, then $\arg[G(\omega)]$ must change by $\geq 3\frac{\pi}{2}$. This violates the phase condition needed to be satisfied, and implies that $p \leq z + 2$. From part 1 of the proof, we have that $p \geq z + 2$, so it must be that p=z+2.

An implication of the above result is that for responses with rational transfer functions, the initial value theorem for Laplace transforms of causal functions (satisfying eq. (5.28)) implies $g(0) = 0$. This is clear by the following argument:

$$g(0) = \lim_{s \to \infty} sG(s) = \lim_{s \to \infty} 1/s = 0 \tag{5.30}$$

precluding a pure exponential of the form $A\exp\left(-\frac{t}{\tau}\right)u(t)$ from being a valid fiber response because it is non-zero at $t = 0$.

Implications for the limiting squeezing become clear. There does not exist a local-oscillator that can take the noise down to 0 asymptotically, at least for the class of fiber responses with rational transfer functions. Once again, we are confronted with the possibility of a floor we cannot remove. This bears resemblance to the CW case non-instanta-

neous response with $\omega \neq 0$. The difference is that here the exact pump profile and the local-oscillator chosen determine the floor. For each pump pulse, the floor can be determined by a maximization of the objective function $\frac{B_2^2}{A_2^2}$. A condition for this maximization can be found by functional differentiation of the objective function, but the resulting condition is non-trivial to solve for the optimal local-oscillator. A more practical method would be to maximize the objective over a subclass of square integrable local-oscillators. A parametric Lagrangian scheme might be suitable for that purpose.

We may also want to know how the rate of approach of the noise-floor depends on the choice of local-oscillator. Just like in the CW case, in which different frequencies had differing rates at which the floor was reached at high Φ_{NL}, similar issues may come up for the pulsed case.

5.2 Specific pulsed excitations

The results from last section can be put on a clear footing by evaluating the full FWM squeezing for some of the pulse excitations that have experimentally been used and comparing the squeezing for different local-oscillators. Agreement between the full FWM results and the limiting cases will confirm the behavior of squeezing at high Φ_{NL}, and help us identify the significance of each term in the approximation.

The most commonly used input to the fiber is a Gaussian pulse, as in the experiments by Bergman and Haus [7]. This presents analytical difficulties with some of the covariance terms in our calculations, but can be numerically evaluated to high accuracy using Fourier transforms instead of time domain computations. The other kind of pulse used as an example here is a single-sided exponential, which is analytically tractable for the most part, and for computations like the noise-floor it has an advantage that clear expressions can be found and examined in various Φ_{NL} regions. Besides, it exhibits a peculiarity that has interesting consequences for the squeezing computations.

We shall continue, in what follows, to absorb the chirp modulation in the local-oscillator. The exponential phase factor of eq. (3.1) will not appear explicitly in what follows.

5.2.1 Gaussian pulse excitation

The Gaussian pump profile is assumed to be:

$$e_{IN}(t) \;=\; \exp\left(-\left(\alpha\frac{\Gamma}{2}t\right)^2\right) \tag{5.31}$$

where α is the width parameter and relates the pump width to the fiber response width. The introduction of normalized parameters in the Haus-Boivin model has suppressed the need to work with the exact experimental values of the response and pulse durations, because in the final analysis Γ cancels out. We choose α to be 0.01 for our calculations to give a 1 ps pulse width compared to a femtosecond width of the response.

Next we consider the terms that need to be computed both for the normally-ordered and the phase-sensitive covariances. First, the normally-ordered terms:

$$\begin{aligned}\Phi_{NL}\int dt\int du\int\frac{d\omega}{2\pi}G_i(\omega)\coth(\hbar\omega/2\mathrm{kT})\cos\left[\omega(t-u)\right]\psi(t)\,\psi^*(u)\\ =\;\Phi_{NL}\int\frac{d\omega}{2\pi}G_i(\omega)\coth(\hbar\omega/2\mathrm{kT})|\Psi(\omega)|^2\end{aligned} \tag{5.32}$$

$$\frac{i}{2}\Phi_{NL}\int dt\int du\left[g(u-t)-g(t-u)\right]\psi(t)\,\psi^*(u) \;=\; -\Phi_{NL}\int\frac{d\omega}{2\pi}G_i(\omega)\,|\Psi(\omega)|^2 \tag{5.33}$$

and then the phase-sensitive terms:

$$\begin{aligned}-\Phi_{NL}\int dt\int du\int\frac{d\omega}{2\pi}G_i(\omega)\coth(\hbar\omega/2\mathrm{kT})\cos\left[\omega(t-u)\right]\psi^*(t)\,\psi^*(u)\\ =\;-\Phi_{NL}\int\frac{d\omega}{2\pi}G_i(\omega)\coth(\hbar\omega/2\mathrm{kT})\Psi^*(-\omega)\,\Psi^*(\omega)\end{aligned} \tag{5.34}$$

$$\begin{aligned}\frac{i}{2}\Phi_{NL}\int dt\int du\left[g(u-t)+g(t-u)\right]\psi^*(t)\,\psi^*(u)\\ =\;i\Phi_{NL}\int\frac{d\omega}{2\pi}G_r(\omega)\,\Psi^*(-\omega)\,\Psi^*(\omega)\end{aligned} \tag{5.35}$$

where $\psi(t)$ is as defined in the last section, $\psi(t) = e_{IN}^*(t)\rho_{LO}(t)$, and

$$\Psi(\omega) = \int dt \psi(t) e^{i\omega t} \tag{5.36}$$

The remaining terms are computed directly in the time domain, and offer no advantage in the frequency domain. In the above, Fourier domain calculations have reduced the number of integrations that need to be performed to two (one for the calculation of the transform itself, assuming it is not known analytically) instead of three. Until now, no mention has been made explicitly of the local-oscillators which will be put to test. Here, we take our cue from the instantaneous case, because the pulse width is large compared to the response decay time, and consider the following three local-oscillators choices:

1. The bright-fringe local-oscillator: Originally proposed by Haus and Shirasaki [6], this is the mean field output of a Mach-Zehnder interferometer that contains in both of its arms the same length of the fiber. It has the following form:

$$\rho_{LO}(t) = \frac{\alpha\Gamma}{\sqrt{2\pi}} \exp\left(-\left(\alpha\frac{\Gamma}{2}t\right)^2\right) e^{i\phi} \tag{5.37}$$

hence the effective local-oscillator is the pump pulse normalized to have energy 1.

2. The pulse-compressed local-oscillator: Proposed by Joneckis and Shapiro [13], this retains the chirped phase like the bright-fringe local-oscillator, but has additional compression in the mean-field term given by the compression parameter β:

$$\rho_{LO}(t) = \frac{\beta\Gamma}{\sqrt{2\pi}} \exp\left(-\left(\beta\frac{\Gamma}{2}t\right)^2\right) e^{i\phi} \tag{5.38}$$

3. The weak-signal FWM local-oscillator: Proposed by Prem-Kumar [28], this local-oscillator is generated by introducing a weak version of the pump signal instead of vacuum into the Mach-Zehnder interferometer of the Haus-Shirasaki configuration, and using the dark fringe output as the local-oscillator. It has additional phase on it in order to imitate the phase of the input fluctuation operator:

$$\rho_{LO}(t) = Ae^{i\phi}\left(\begin{array}{c} e_{IN}(t)\,e^{i\theta} + i\Phi_{NL}\int g(t-\tau)\,e_{IN}{}^{*}(\tau)\,e_{IN}(\tau)\,e^{i\theta}e_{IN}(t)\,d\tau \\ + i\Phi_{NL}\int g(t-\tau)\,e_{IN}(\tau)\,e_{IN}{}^{*}(\tau)\,e^{-i\theta}e_{IN}(t)\,d\tau \end{array}\right) \tag{5.39}$$

where the constant A is introduced as the normalization coefficient, as the weak-signal FWM local-oscillator does not have an analytical form for a general response $g(t)$. The first two local-oscillators can be analytically evaluated, at least to the point of evaluation of eq. (5.36). After that, numerical computations are called upon. The weak-signal FWM local-oscillator is also tackled with the help of Fourier transform, but it is a bit trickier, and needs numerics to begin with.

5.2.1.1 Instantaneous interaction noise characteristics

We present the Gaussian pump, instantaneous interaction results first which are analytically calculated from the results of section 1.3 (eq. (1.27)). Fig. 5.1 shows the comparison of several local-oscillators. Evidently, the bright-fringe local-oscillator is far from optimal, both because it misses the point of maximum squeezing at the peak of the pump input, and has the incorrect phase at all times. As the phase is corrected by the choice of weak-signal FWM local-oscillator, squeezing improves dramatically and no longer displays the floor that the bright-fringe local-oscillator did. We can examine this difference in performance if we set $\theta = 0$ in eq. (5.39), and compute the weak-signal local-oscillator for the instantaneous response, $h(t) = \kappa\delta(t)$:

$$\rho_{LO}(t) = Ae^{i\phi}\left[1 + 2i\Phi_{NL}\left|e_{IN}(t)\right|^2\right]e_{IN}(t) \tag{5.40}$$

where:

$$A = \left(\int dt\left|e_{IN}(t)\right|^2 + 4\Phi_{NL}^2\int dt\left|e_{IN}(t)\right|^4\right)^{-1/2} \tag{5.41}$$

$\rho_{LO}(t)$ of eq. (5.40) simplifies for the Gaussian pump of (5.31) to:

$$\rho_{LO}(t) = \sqrt{\alpha\frac{\Gamma}{2}}\left(\frac{1}{\sqrt{2}}+\frac{4\Phi_{NL}^2}{\sqrt{6}}\right)^{-1/2} e^{i\phi}\left[1+2i\Phi_{NL}\exp\left(-2\left(\alpha\frac{\Gamma}{2}t\right)^2\right)\right]\exp\left(-\left(\alpha\frac{\Gamma}{2}t\right)^2\right) \tag{5.42}$$

from which eq. (1.27) becomes:

$$\sigma_N^2 = 1+2\left(\frac{1}{\sqrt{2}}+\frac{4\Phi_{NL}^2}{\sqrt{6}}\right)^{-1}\left\{\begin{array}{c}\Phi_{NL}^2\left(\frac{1}{\sqrt{6}}+\frac{4\Phi_{NL}^2}{\sqrt{10}}\right)\\ -\left|\Phi_{NL}\left(\frac{1}{2}\right)-i\Phi_{NL}^2\left(\frac{3}{\sqrt{6}}+\frac{4\Phi_{NL}^2}{\sqrt{10}}\right)\right|\end{array}\right\} \tag{5.43}$$

This has an asymptotic expansion of:

$$\frac{1}{4}(\sqrt{3})/\Phi_{NL}^2+\left(-\frac{\sqrt{15}+6}{32}\right)/\Phi_{NL}^4+\text{- - - -} \tag{5.44}$$

which lacks a constant term, i.e., the noise-floor. The factor of $\sqrt{3}$ in the leading term spells the squeezing under-performance of ≈ 2.4 dB compared to the instantaneous interaction result infinite pulse-compression result of chapter 1 (eq. (1.34)) in which the leading term in the asymptotic expansion is $\frac{1}{4\Phi^2_{NL}}$.

Further improvements come about if pulse-compressed local-oscillators are chosen, and higher degrees of compression lead to lower floors. Our explanations succeeding eq. (1.30) suffice to establish the optimality of an infinitely compressed local-oscillator. We have included in Fig. 5.1 the floor values for the bright-fringe and pulse-compressed local-oscillators, calculated from the following expression:

$$10.\log_{10}\left(1-\frac{\sqrt{2}\beta\sqrt{4\alpha^2+2\beta^2}}{2\alpha^2+2\beta^2}\right) \tag{5.45}$$

which testifies to the fact that the floor disappears for $\beta\rightarrow\infty$. We note from Fig. 5.1 that local-oscillators compressed to a higher extent bound the performances of those with lesser degrees of compression, with the exception that the weak-signal local-oscillator does better at noise reduction than the bright-fringe local-oscillator although they have the same pulse widths. A look at eq. (5.42) reveals that the weak-signal local-oscillator only

differs from the bright-fringe local-oscillator in its phase at each time instant, and this choice of phase makes it superior to the bright-fringe local-oscillator at each Φ_{NL}, as well as helps to remove the high Φ_{NL} floor that plagues the pulse-compressed local-oscillators with unadjustable phases. Next we turn towards the non-instantaneous interaction.

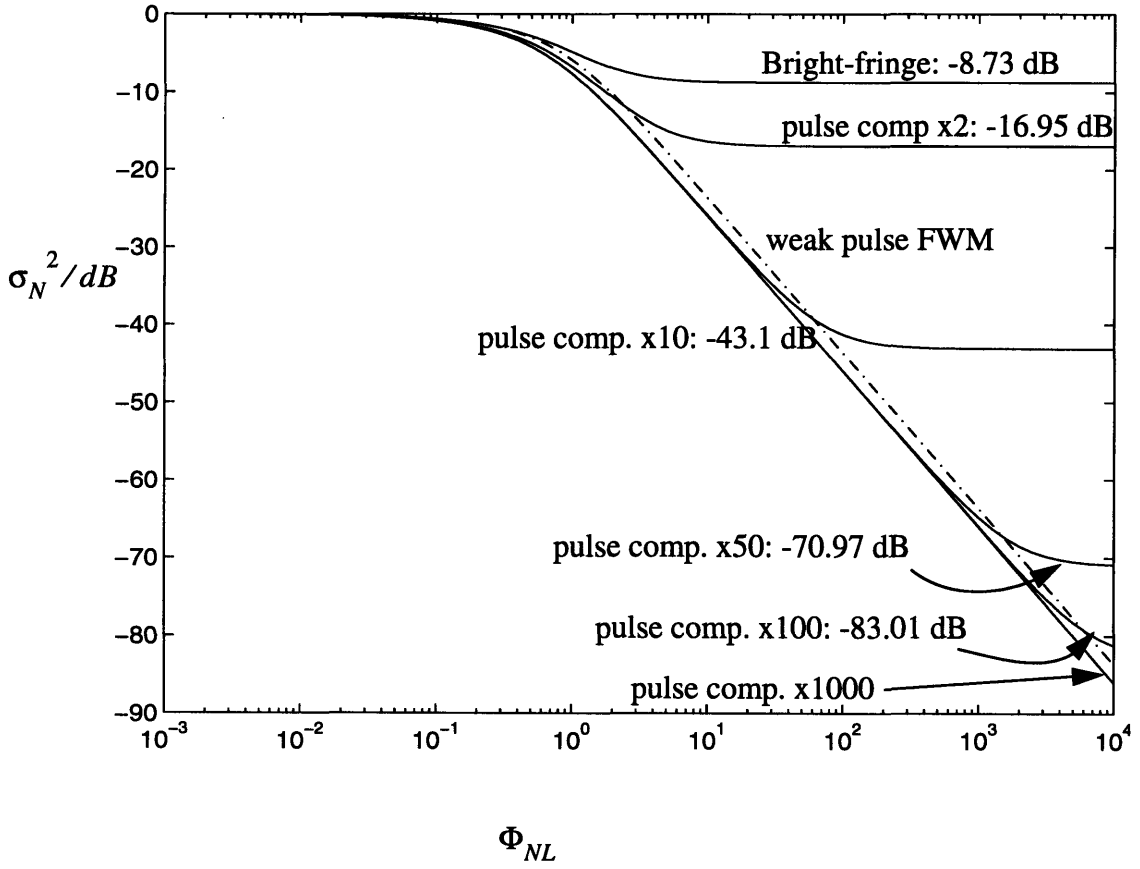

Fig. 5.1 Normalized charge variance vs. nonlinear phase-shift for instantaneous interaction and a Gaussian pump: comparison of different local-oscillators.

5.2.1.2 Non-instantaneous interaction noise characteristics

Fig. 5.2 compares the performances of different local-oscillators. The computations in this figure are for noise levels at absolute zero temperature. We see a performance-spread in the non-instantaneous case.

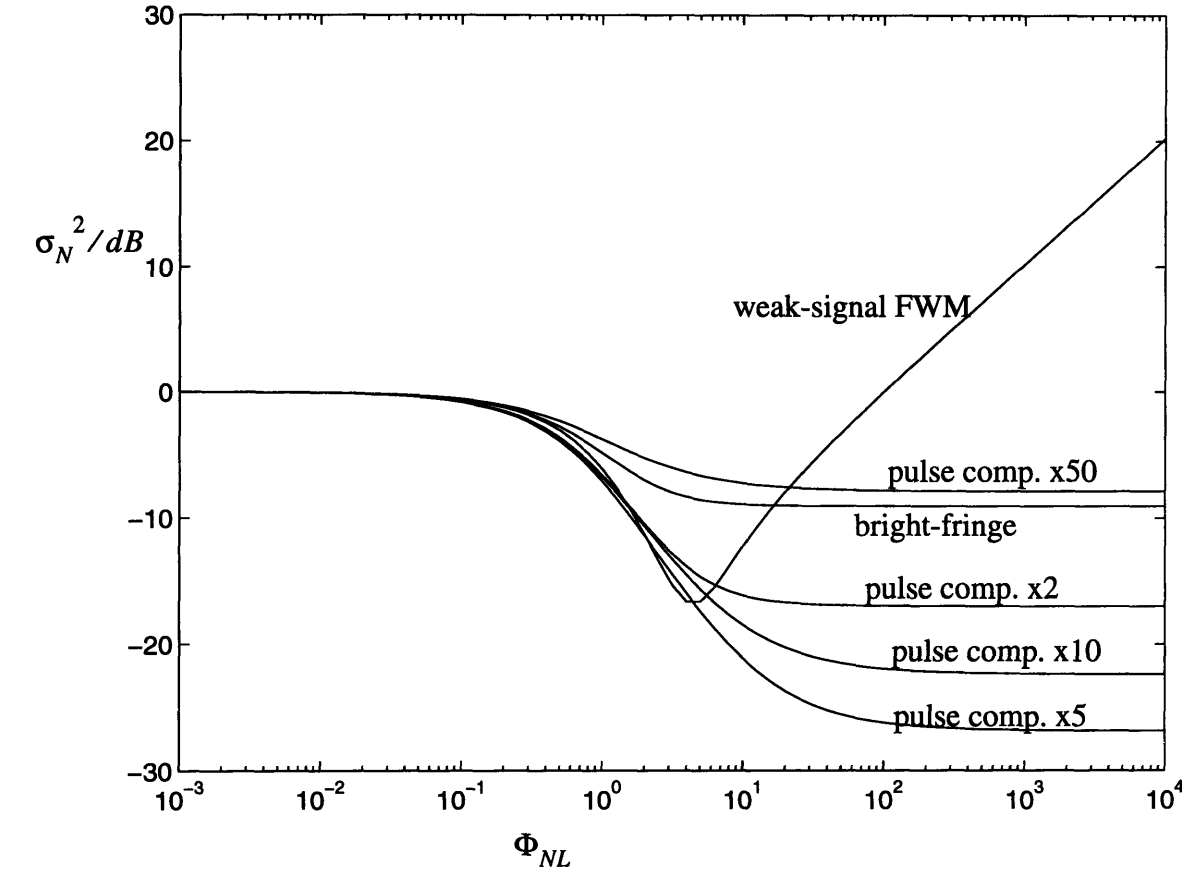

Fig. 5.2 Normalized charge variance vs. nonlinear phase-shift for non-instantaneous interaction (two-pole response) and a Gaussian pump: comparison of different local-oscillators.

There is no monotonicity of local-oscillator capability here, unlike the behavior seen in instantaneous case. For low Φ_{NL}, the weak-signal FWM local-oscillator lies between the bright-fringe and the pulse-compressed local-oscillators. At moderate Φ_{NL} it outperforms both the bright-fringe and the pulse-compressed local-oscillators. At higher phase-shifts, the pulse-compressed local-oscillators begin to exceed the weak-signal FWM local-oscillator performance. Eventually weak pulse FWM local-oscillator reaches a minimum after which its performance degrades rapidly and goes above the shot-noise level. The pulse-compressed local-oscillators, however, smoothly flatten out to noise-floors.Another highly interesting fact is that the pulse-compression only goes so far to improve squeez-

ing. When $\beta \approx 5$ the compression attains its maximum squeezing at -27 dB approximately. At lower and higher compressions, the performance is less impressive.

We can certainly see where the maximum correlations exist in the signal output of the fiber. Usually the pump pulses launched into a fiber have a width of the order of picoseconds. The nonlinear interaction response time is of the order of femtoseconds. The kernel matrix, eq. (5.4), with a product term containing the pump pulse cannot have significant correlations at time separations of more than a pump width. So a local-oscillator much wider than the pump cannot be optimal. Using a local-oscillator whose duration is shorter than that of the fiber response is also not beneficial, because then we risk missing the peak of the term:

$$\frac{i}{2}L\,[\,h\,(u-t)\,+h\,(t-u)\,]\,E_{IN}\,(t)\,E_{IN}\,(u) \tag{5.46}$$

in the phase-sensitive covariance, eq. (5.3). This term provides the difference between the normally-ordered and the phase-sensitive covariances for a real pump and a real local-oscillator, and has a strong effect on the squeezing performance.

We can relate our observations to the CW analysis of chapter 4. For any Φ_{NL} and a given pump, frequency mixing in the fluctuations (as described at the beginning of the chapter) causes the fluctuations to be correlated in frequency, unlike the CW spectrum in which fluctuations at different frequencies were uncorrelated. To exploit these correlations we have to employ a local-oscillator with a finite bandwidth rather than a CW local-oscillator. But a local-oscillator which has a very wide bandwidth also runs into difficulties with the finite bandwidth of the optical nonlinearity and the presence of Raman noise at high frequencies. At very high frequencies, the squeezing in Fig. 4.2 is very weak, both because $G_r\,(\omega)$ is small, and because the peaking Raman gain introduces extra noise. A narrow local-oscillator (wide bandwidth) would sample the high frequencies and therefore have less squeezing than the local-oscillators that have their frequency content in the flat

part of $G_i(\omega)$. The optimal local-oscillator would, consequently, have to be of finite extent in frequency and in time.

For constrained local-oscillator optimizations, in which we optimize the width-parameter for local-oscillators of a particular pulse shape (e.g. Gaussian), this can be an important consideration. Besides the width of the local-oscillator, its phase is also very critical in squeezing calculations.

Comparing the bright-fringe and the weak-signal FWM local-oscillator, we notice a key difference. For the real pump pulse assumed (eq. (5.31)), weak-signal local-oscillator (eq. (5.39)) reduces to:

$$\rho_{LO}(t) = Ae^{i\phi}\left(e^{i\theta} + 2i\Phi_{NL}\cos(\theta)\int d\tau g(t-\tau)\left|e_{IN}(\tau)\right|^2\right)e_{IN}(t) \tag{5.47}$$

which differs from the bright-fringe local-oscillator in the time-dependent phase with which the weak-signal FWM local-oscillator modulates the pump pulse. The input phase θ, which determines the interaction of the pump with the weak-signal through the nonlinear medium, can be adjusted to optimize the time-dependent local-oscillator phase, in addition to the phase ϕ that the homodyne detector appends. As a first cut, we have taken this phase to be 0, for the numerics involved in our computations do not allow optimization over θ. At low Φ_{NL} the coefficient of Φ_{NL} in a σ_N^2 Taylor expansion dominates the squeezing, compared to that of Φ_{NL}^2, and that coefficient is sensitive to proper phase selection of the local-oscillator (see eq. (5.46)). For the weak-signal FWM local-oscillator the particular phase we chose through eq. (5.47) leads to a squeezing performance far superior to the bright-fringe local-oscillator.

Another problem with a non-instantaneous response compared to an instantaneous one is that the low Φ_{NL} range is also affected relatively strongly by the Raman noise sources, so any significant gains that could have come about because of the phase compensation are "screened" out.

At high nonlinear phase-shifts, where the squeezing saturation is seen to occur, a different trend is seen. The weak-signal FWM local-oscillator shoots up and rapidly exceeds the shot-noise level whereas the bright-fringe and the pulse-compressed local-oscillators hold their levels. We immediately see the connection to eq. (5.14) which bars an optimal local-oscillator from having a time-varying phase other than that predicted by the solution of the eq. (2.15) for the kernel matrix of eq. (5.4). There is always some time-dependent phase on the weak-signal FWM local-oscillator. At high Φ_{NL}, it allows the Φ_{NL}^2 term to drive the noise level above the shot-noise value.

5.2.1.3 Analysis of the effect of pulse compression on squeezing

Let us try to quantify the first point about the pulse-compressed local-oscillator having an optimal degree of compression. To show that there is an optimal local-oscillator somewhere between the limiting cases of a very narrow and a very broad pulse, we refer to eqs. (5.17)-(5.19). The noise-floor is $1-\frac{B^2}{A_2^2}$, and as the local-oscillator width is varied we can see its effect on the floor. We limit our treatment here to Gaussian local-oscillators, but it can be generalized to arbitrary local-oscillator shapes.

First, consider a very broad Gaussian local-oscillator pulse of width τ_l:

$$\rho_{LO}(t) = \left(\frac{\sqrt{2}}{\tau_l\sqrt{\pi}}\right)^{1/2} \exp\left(-\left(\frac{t}{\tau_l}\right)^2\right) e^{i\phi} \tag{5.48}$$

Now let us consider the limit in which τ_l is much larger than the width of the pump pulse. The term in the numerator, B in eq. (5.18) becomes:

$$B \approx \frac{\sqrt{2}}{\tau_l\sqrt{\pi}} \int du \int dt e_{IN}(t)\, g_e(t-u)\, e_{IN}(u) \tag{5.49}$$

and the term in the denominator, A_2^2, eq. (5.17) is:

$$A_2^2 \approx \frac{\sqrt{2}}{\tau_l \sqrt{\pi}} \int du \left(\int dt g(t-u)\, e_{IN}(t) \right)^2 e_{IN}^2(u) \tag{5.50}$$

therefore

$$\frac{B^2}{A_2^2} \approx \frac{\sqrt{2}}{\tau_l \sqrt{\pi}} \frac{\left(\int du \int dt e_{IN}(t)\, g_e(t-u)\, e_{IN}(u) \right)^2}{\int du \left(\int dt g(t-u)\, e_{in}(t) \right)^2 e_{IN}^2(u)} \propto \frac{1}{\tau_l} \tag{5.51}$$

which asymptotically goes to 0 at large pulse-widths. The noise-floor thus rises up to the shot-noise level.

The opposite extreme of a very narrow local-oscillator can also be analyzed similarly. We assume a narrow width Gaussian local-oscillator parametrized by a width parameter τ_l, and a double-sided, i.e., a symmetric pump, the reasons for which will become clear shortly:

$$\rho_{LO}(t) = \zeta_{LO}(t)\, e^{i\phi} = \left(\frac{\sqrt{2}}{\sqrt{\pi}\tau_l} \right)^{\frac{1}{2}} \exp\left(-\left(\frac{t}{\tau_l} \right)^2 \right) e^{i\phi} \tag{5.52}$$

which, because of the condition (1.28), in the limit $\tau_l \ll 1$ becomes an impulse of the form:

$$\zeta_{LO}(t) \approx \left(\sqrt{2\pi}\tau_l \right)^{\frac{1}{2}} \delta(t) \tag{5.53}$$

We have to resort to an approximation which takes into account the vanishing of $g(0)$. We define new variables:

$$t_+ = \frac{t+u}{2} \tag{5.54}$$

and

$$t_- = t-u \tag{5.55}$$

in terms of which B becomes:

$$B = \int dt_{-} g_e\left(t_{-}\right) \int dt_{+} e_{IN}\left(t_{+} + \frac{t_{-}}{2}\right) e_{IN}\left(t_{+} - \frac{t_{-}}{2}\right) \zeta_{LO}\left(t_{+} + \frac{t_{-}}{2}\right) \zeta_{LO}\left(t_{+} - \frac{t_{-}}{2}\right) \tag{5.56}$$

and under the assumption of a very narrow local-oscillator we can assume that the pump remains constant over the local-oscillator duration:

$$B \approx e_{IN}^2(0) \int dt_{-} g_e\left(t_{-}\right) R_{\zeta\zeta}\left(t_{-}\right) = 2e_{IN}^2(0) \int_0^{\infty} dt_{-} g\left(t_{-}\right) R_{\zeta\zeta}\left(t_{-}\right) \tag{5.57}$$

where $R_{\xi\xi}\left(t_{-}\right)$ is the even, positive-definite auto-correlation over time of the local-oscillator $\xi_{LO}(t)$:

$$R_{\zeta\zeta}\left(t_{-}\right) = \int dt_{+} \zeta_{LO}\left(t_{+} + \frac{t_{-}}{2}\right) \zeta_{LO}\left(t_{+} - \frac{t_{-}}{2}\right) \tag{5.58}$$

$g(t)$ can be expressed as its series expansion for $t \geq 0$ as:

$$g(t) = g(0) + t g'\left(0^{+}\right) + \text{- - - - - - - - -} \tag{5.59}$$

which is substituted in eq. (5.57) with $g(0) = 0$ to yield:

$$B \approx 2e_{IN}^2(0) \int_0^{\infty} dt_{-} t_{-} g'\left(0^{+}\right) R_{\zeta\zeta}\left(t_{-}\right) \tag{5.60}$$

For a Gaussian local-oscillator eq. (5.58) can be evaluated to:

$$R_{\zeta\zeta}\left(t_{-}\right) = \exp\left(-2\left(\frac{t_{-}}{2\tau_l}\right)^2\right) \tag{5.61}$$

for which eq. (5.60) simplifies [29] to:

$$B \approx e_{IN}^2(0)\, g'\left(0^{+}\right) \sqrt{2} \tau_l^2 \tag{5.62}$$

We can also simplify A_2^2 in the narrow local-oscillator limit:

$$A_2^2 \approx \int d\tau \left(\left(\sqrt{2\pi}\tau_l \right)^{\frac{1}{2}} \int dt \delta(t)\, g(t-\tau)\, e_{IN}(t) \right)^2 e_{IN}^2(\tau)$$
$$= \sqrt{2\pi}\tau_l \int d\tau g^2(-\tau)\, e_{IN}^2(\tau) \tag{5.63}$$

implying:

$$\frac{B^2}{A_2^2} \approx \sqrt{\frac{2}{\pi}}\tau_l \frac{\left(e_{IN}^2(0) \left[g'\left(0^+ \right) \right] \right)^2}{\int dt g^2(-t)\, e_{IN}^2(t)} \tag{5.64}$$

So with very narrow Gaussian pump and local-oscillators, the ratio $\frac{B^2}{A_2^2} \propto \tau_l^3$, and just as in eq. (5.51) the noise-floor rises up to the shot-noise level. The assumption of a symmetric pump, $e_{IN}(t) = e_{IN}(-t)$, comes into play here. It ensures that we have captured the leading term in the $\tau_l \to 0$ expansion of A_2^2.

Likewise we can find the effect of extreme local-oscillator widths on the $\frac{1}{\Phi_{NL}}$ coefficient in the expansion (5.19). That coefficient is:

$$\frac{B^2 A_1}{A_2^4} \tag{5.65}$$

but $\frac{B^2}{A_2^4}$ is a constant for very wide local-oscillator and for very narrow local-oscillator it is:

$$\frac{B^2}{A_2^4} \propto \tau_l^2 \tag{5.66}$$

From above computations, A_1 (see eq. (5.16)) goes as:

$$A_1 \approx \tau_l e_{IN}^2(0) \frac{1}{\sqrt{2\pi}} \int d\omega G_i(\omega) \coth(\hbar\omega/2kT) \tag{5.67}$$

for a narrow local-oscillator, and as:

$$A_1 \approx \frac{\sqrt{2}}{\tau_l \sqrt{\pi}} \int \frac{d\omega}{2\pi} G_i(\omega) \coth(\hbar\omega/2kT) \left| \tilde{e}_{IN}(\omega) \right|^2 \tag{5.68}$$

for a very wide local-oscillator.

where $\tilde{e}_{IN}(\omega) = \int dt e_{IN}(t)\, e^{i\omega t}$.

From eqs. (5.67) and (5.68) it is clear that:

$$\frac{B^2 A_1}{A_2^4} \propto \tau_l^3 \tag{5.69}$$

for a narrow local-oscillator and,

$$\frac{B^2 A_1}{A_2^4} \propto \frac{1}{\tau_l} \tag{5.70}$$

for a wide local-oscillator. The rate at which the floor is approached is, therefore, speeded up if the local-oscillator is very narrow or very wide. Moreover, because the noise-floors increase as $\tau_l \to 0$ or $\tau_l \to \infty$, we see that these floors dominate the narrow and wide local-oscillator limits. The optimal local-oscillator therefore lies somewhere between the two extremes.

5.2.2 Single-sided exponential excitation

This pump has the form:

$$e_{IN}(t) = \exp\left(-\alpha\frac{\Gamma}{2}t\right)u(t) \tag{5.71}$$

where we are once again adopting normalized pulse widths through α, chosen to make the pulse width 1 ps. The various local-oscillator performances are plotted in Fig. 5.3. Again, the temperature is assumed to be absolute zero.

We see something curious here. The floor keeps decreasing with higher local-oscillator compression. This is quite peculiar considering we said earlier that at high pulse-compressions the noise-floor should recede to the shot-noise level. The conflict can be resolved by noticing that for the derivation in the Gaussian case, we assumed a double-sided smoothly

varying pump shape for eq. (5.63). Here, that has changed because of the step change in the pump and local-oscillators at t=0. Eq. (5.63) has to be examined for the next order term in its expansion now. Fortunately we have the exact noise-floor expression in terms of pump and local-oscillator widths and do not need to approximate.

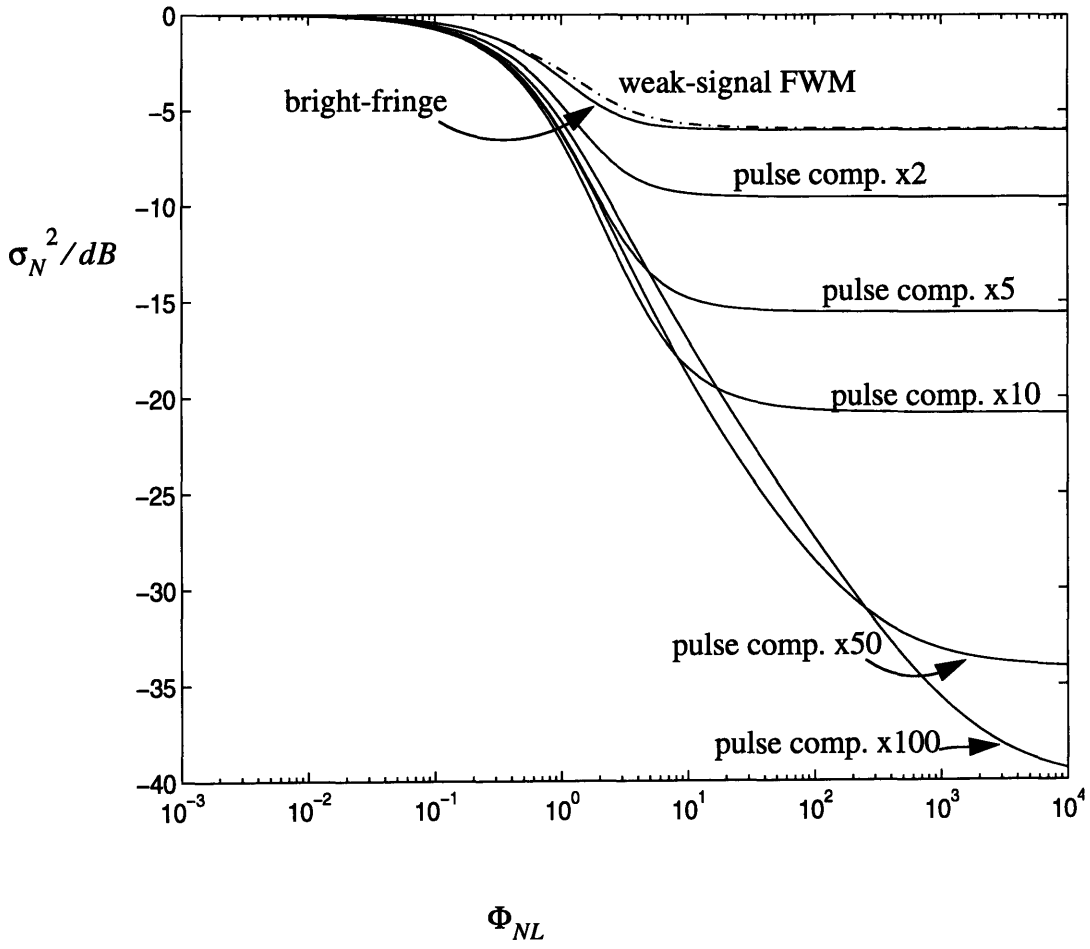

Fig. 5.3 Normalized charge variance vs. nonlinear phase-shift for non-instantaneous interaction (two-pole response) and a single-sided exponential pump: comparison of different local-oscillators.

The single-sided exponential pump has a duration of τ_p seconds:

$$e_{IN}(t) = \exp\left(-\frac{t}{\tau_p}\right)u(t) \tag{5.72}$$

and the local-oscillator has the same form and a duration of τ_l seconds:

$$\zeta_{LO}(t) = \sqrt{\frac{2}{\tau_l}}\exp\left(-\frac{t}{\tau_l}\right)u(t) \tag{5.73}$$

Then the floor calculations, assuming the two-pole response, reveal:

$$1-\frac{B^2}{A_2^2} = \left(\frac{\frac{\tau_l}{\tau_p}}{1+\frac{\tau_l}{\tau_p}}\right)^2 \tag{5.74}$$

goes to 0 as $\tau_l \to 0$.

We also notice that at moderate Φ_{NL} squeezing does not improve continuously with local-oscillator compression. Just as in the Gaussian pump case, there is an optimal local-oscillator width after which noise levels begin to rise. Since the noise-floor must decline with the compression, it is primarily the $\frac{1}{\Phi_{NL}}$ term that determines the noise variation at high Φ_{NL}. The distinguishing feature of the single-sided exponential pump is brought out in the coefficient of $\frac{1}{\Phi_{NL}}$ in the expansion (5.19).

5.2.2.1 Analysis of the effect of pulse compression on squeezing

We omit the case of very broad local-oscillator for which the Gaussian results hold. For the narrow local-oscillator, our analysis follows the general lines along which the Gaussian case was studied, with a highly compressed local-oscillator:

$$\zeta_{LO}(t) = \sqrt{\frac{2}{\tau_l}}\exp\left(-\frac{t}{\tau_l}\right)u(t) \tag{5.75}$$

which, because of the condition (1.28), in the limit $\tau_l \ll 1$ takes the impulse-like form:

$$\zeta_{LO}(t) \approx \sqrt{\frac{\tau_l}{2}}\delta(t) \tag{5.76}$$

Evaluating eq. (5.58) we find:

$$R_{\zeta\zeta}\left(t_-\right) = \exp\left(-\left|\frac{t_-}{\tau_l}\right|\right) \tag{5.77}$$

and upon substitution into eq. (5.60) we obtain:

$$B \approx 2g'\left(0^+\right)\tau_l^2 \tag{5.78}$$

where we have used: $e_{IN}(0) = 1$. Of critical importance is the fact that the ratio $\frac{B^2}{A_2^2}$ tends towards 1 as the local-oscillator gets narrower. Instead of having to explicitly approximate A_2^2 from eq. (5.58) (although we have the exact expression for it, used to generate the floor in eq. (5.74)), we use the relation $B^2 \approx A_2^2$ in the limit $\tau_l \ll 1$. This relation implies:

$$\frac{B^2 A_1}{A_2^4} \approx \frac{A_1}{B^2} \tag{5.79}$$

which in turn gives, from the exponential version of eq. (5.68):

$$A_1 \approx \frac{\tau_l}{2} e_{IN}^2(0) \int dt \int du \frac{1}{2\pi} \int d\omega G_i(\omega) \coth(\hbar\omega/2kT) \tag{5.80}$$

and, via eq. (5.78)):

$$\frac{B^2 A_1}{A_2^4} \approx \frac{\int \frac{d\omega}{2\pi} G_i(\omega) \coth(\hbar\omega/2kT)}{8\left[g'\left(0^+\right)\right]^2 \tau_l^3} \tag{5.81}$$

We can evaluate, from eq. (3.7), $g'\left(0^+\right)$ for the two-pole response as:

$$g'\left(0^+\right) = \Omega^2 \tag{5.82}$$

which is substituted in eq. (5.81) to yield:

$$\frac{B^2 A_1}{A_2^4} \approx \frac{\int \frac{d\omega}{2\pi} \frac{\Omega^2 \omega \Gamma}{\left(\Omega^2 - \omega^2\right)^2 + \omega^2 \Gamma^2} \coth(\hbar\omega/2kT)}{8\Omega^4 \tau_l^3} \tag{5.83}$$

Eq. (5.83) further simplifies if we make an order of magnitude approximation of the numerator by recognizing that at T=0, $\coth(\hbar\omega/2kT) = 1$ for $\omega > 0$ and that the integrand is an even function of ω. We are assisted in completing the approximation if we remember that $G_i(\omega)$ is highly peaked at the resonance frequency Ω, and decays sharply to small values within a width of 2Γ. To the first order then, it is a triangle of area $\frac{\Omega}{2\pi}$. The resultant expression for eq. (5.83) is:

$$\frac{B^2 A_1}{A_2^4} \approx \frac{1}{16\pi\Omega^3 \tau_l^3} \tag{5.84}$$

whereby the coefficient of $\frac{1}{\Phi_{NL}}$ is seen to blow up as smaller τ_l are chosen. There is a strong effect of this term on the onset of the high Φ_{NL} regime. It takes much higher Φ_{NL} to get to the floor of the noise curves for smaller τ_l because the coefficient of $\frac{1}{\Phi_{NL}}$ prevails in guiding the noise behavior until then. As we look at regimes away from the noise-floor, successive terms in the approximation have greater influence on the noise.

We are left with the conclusion that the disappearance of noise-floor with higher compression of the local-oscillator is accompanied with a slower approach to the floor. Indeed as eq. (5.84) shows, an infinitely narrow local-oscillator, will not yield $\sigma_N^2 \to 0$.

The third case of interest, the weak-signal FWM local-oscillator now has a floor within the Φ_{NL} regime shown. This is the result of the particular form of the pump and the local-oscillator chosen. They both have exponential dependence just like the two-pole fiber response. At the Φ_{NL} plotted, the local-oscillator exactly compensates the effect of any incremental change in Φ_{NL}^2 by a corresponding change in its own phase, hence preventing the noise explosion from happening. Unlike the instantaneous response, however,

the floor does not disappear entirely, but only reaches a level very close to that of the bright-fringe local-oscillator. We can relate this to the expression for weak-signal FWM local-oscillator of eq. (5.47). At low Φ_{NL}, the time-varying phase adversely affects the noise, maintaining it over the bright-fringe noise level. At higher Φ_{NL} the phase of the weak-signal FWM local-oscillator is very close to $\frac{\pi}{2}$ from the Φ_{NL} term, which is essentially a convolution of a single-sided exponential with the two-pole response. The weak-signal local-oscillator steadily evolves towards a constant phase signal with a pulse width the same as the bright-fringe local-oscillator, hence the convergence in their performances. It is due to the two-pole response function chosen that the phase of the local-oscillator (derived from a weak single-sided exponential signal through the FWM interaction eq. (5.47)) adjusts such that increments in Φ_{NL}^2 (eq. (5.14)) are counteracted by a corresponding decrease in its coefficient. As a result noise is kept from overshooting the shot-noise level.

We conclude this chapter with some speculations to account for the apparent discrepancy between the instantaneous and non-instantaneous interaction, specially in connection with the weak-signal FWM local-oscillator. We have encountered three distinct noise characteristics for the cases we have studied. The weak-signal FWM local-oscillator succeeded in removing the noise-floor for the instantaneous interaction (eq. (5.44)) example. On the other hand, for the non-instantaneous interaction, it leveled the noise to a floor for the single-sided exponential pump, and made the noise depart towards and eventually above the shot-noise level for the Gaussian pump.

These observations re-emphasize our contention that a local-oscillator desired to behave optimally at high Φ_{NL} must *tend* towards a constant phase function. The weak-signal FWM local-oscillators for the instantaneous and the non-instantaneous cases adjust their phases to approach a constant phase as Φ_{NL} grows. But there is more to the picture than that. It is of critical importance how that constant phase is reached. In the non-instantaneous interaction Gaussian pump case, the weak-signal FWM local-oscillator could not

adjust its phase rapidly enough to overcome the growing Φ_{NL}^2 term, resulting in a noise that could not be contained below the shot-noise level. The single-sided exponential managed to reduce the noise to a floor, but was unable to do better, lending credibility to our earlier statement that the two-pole response is inherently immune to any attempts at removing the floor. The case of instantaneous interaction underscores the as yet unstated side of our presentation, i.e., there may be more than one trajectory along which local-oscillators can be chosen to defeat the noise-floor. The weak-signal FWM local-oscillator is one such proposed form, but there are other such local-oscillators like the phase-optimized one used in chapter 1, to arrive at eq. (1.29), that also get rid of the floor.

Finally, a word of caution. The asymptotic expansion we chose as a vehicle to carry forward our investigation of the noise behavior, though insightful with regards to the limiting form of a local-oscillator, is only circumspect about the optimal local-oscillator *per se*. For those fiber responses which allow the noise-floor to be removed, an optimal local-oscillator will surely do the same, but every local-oscillator that removes the noise-floor is not optimal. One has to go beyond the expansion and actually solve the integral equation (2.16) with the kernel of eq. (5.4) to get the optimal local-oscillator, as mentioned earlier.

Chapter 6

Local-Oscillator Optimization for a Spatial FWM interaction: Gaussian Spatial Response.

We finally shift our focus away from the time-dependent FWM case that we have been probing until now, and generalize our work to discuss a plausible spatial variation in the nonlinear interaction over the fiber cross-section. This idea is inspired by the work of Prem Kumar *et al.* [20] who have investigated the diffractive effects in three wave mixing (TWM) interaction in an optical parametric amplifier. Since the intent of this chapter is mainly to demonstrate that generalizations can be handled within the optimization framework of chapter 2, and to explicitly obtain the eigenvalues and eigenfunctions for a spatial response, we assume that the temporal interaction is instantaneous, hence affording us the convenience of optimizing solely over the spatial coordinates. We specialize our work to an FWM approximation in the spatial interaction of the field with the fiber, instead of the TWM that Prem Kumar *et al.* [20] considered.

6.1 Model assumptions and framework development

We borrow from the chapter 2 formalism, with a modification that the current operator $\hat{i}(t)$ is replaced by a current density operator $\hat{j}(\vec{r}, t)$, where $\vec{r} = (x, y)$ is the spatial position on the detector surface. $\hat{i}(t)$ and $\hat{j}(\vec{r}, t)$ are related by:

$$\hat{i}(t) = \int_A d\vec{r}\,\hat{j}(\vec{r}, t) \tag{6.1}$$

where A is the surface area of the detector and the integral is over the spatial coordinates. The current density, $\hat{j}(\vec{r}, t)$, for balanced homodyne detection is expressible in terms of the signal field as:

$$\hat{j}(\vec{r}, t) = 2qRe\left[\hat{E}_S(\vec{r}, t)\, E_{LO}{}^*(\vec{r})\right] \tag{6.2}$$

for a strong CW coherent-state local-oscillator with classical spatial field $E_{LO}(\vec{r})$.

In this expression, the signal field satisfies:

$$[\hat{E}_S(\vec{r}, t), \hat{E}_S(\vec{v}, u)] = 0 \qquad \left[\hat{E}_S(\vec{r}, t), \hat{E}_S{}^{\dagger}(\vec{v}, u)\right] = \delta(\vec{r} - \vec{v})\,\delta(t - u) \tag{6.3}$$

To simplify matters even further, we assume that the pump is CW, hence allowing us to work in the frequency domain directly, as in eq. (4.2). We shall assume a spatial Kerr-effect interaction with a spatial impulse response, which we shall denote $g(\vec{r})$. To reduce the optimization to a 1-D calculation, we shall assume that the pump field profile as well as the spatial response are varying in the x-direction and centered around $\vec{r} = 0$, with no y-dependence.

Finally, we shall assume that $g(\vec{r})$ is symmetric in the x-direction. Because this is not a temporal response, causality is not an issue. Spatial symmetry is both physically reasonable, and obviates the need for Raman noise to preserve commutator brackets.

We can easily consider the zero frequency spectrum for optimization, as the signal will now be a stationary white-noise, and the only variation left to be dealt with is the spatial one. In direct analogy to the temporal case of chapter 2, we introduce zero frequency normally-ordered and phase-sensitive spatial covariances with respect to the x coordinate:

$$S^{(p)}(x, x') = \langle \Delta\hat{E}_S(x)\, \Delta\hat{E}_S(x') \rangle \qquad S^{(n)}(x, x') = \langle \Delta\hat{E}_S{}^{\dagger}(x)\, \Delta\hat{E}_S(x') \rangle \tag{6.4}$$

and write the normalized zero-frequency current spectrum as:

$$\begin{aligned} S_N &= 1 + 2\int dx \int dx' S^{(n)}(x, x')\, \xi_{LO}(x)\, \xi_{LO}{}^*(x') \\ &\quad + 2Re\int dx \int dx' S^{(p)}(x, x')\, \xi_{LO}{}^*(x)\, \xi_{LO}{}^*(x') \end{aligned} \tag{6.5}$$

where $\xi_{LO}(x)$ is the x-normalized local-oscillator field: $\int dx |\xi_{LO}(x)|^2 = 1$.

The kernel matrix for eq. (6.4) is now given by:

$$S(x,x') = \left[\begin{array}{c|c} S_R^{(p)}(x,x') + S_R^{(n)}(x,x') & S_I^{(n)}(x,x') + S_I^{(p)}(x,x') \\ \hline S_I^{(p)}(x,x') - S_I^{(n)}(x,x') & S_R^{(n)}(x,x') - S_R^{(p)}(x,x') \end{array}\right] \tag{6.6}$$

with the subscripts I and R representing the real and imaginary parts of the covariance functions. Thus eq. (6.5) becomes:

$$S_N = 1 + 2\int dx \int dx' \gamma(x)^T S(x,x') \gamma(x') \tag{6.7}$$

where:

$$\gamma(x) = \begin{bmatrix} Re\{\xi_{LO}(x)\} \\ Im\{\xi_{LO}(x)\} \end{bmatrix} \tag{6.8}$$

6.2 Optimal spatial local-oscillator description

To get the optimal local-oscillator, the integral equation to be solved is:

$$\int dv S(x,x') \Phi_i(x') = \lambda_i \Phi_i(x) \tag{6.9}$$

$$\int dr \Phi_i(x)^T \Phi_j(x) = \delta_{ij} \tag{6.10}$$

The minimum noise spectrum is related to the minimum eigenvalue λ_{min} by:

$$S_N = 1 + 2\lambda_{min} \tag{6.11}$$

and the optimal local-oscillator in its two-dimensional form is the eigenfunction Φ_{min} to which the eigenvalue λ_{min} belongs.

6.3 Spatio-temporal FWM model

Our model suggests a natural generalization of the non-instantaneous interaction FWM to a spatial variation. With the exclusion of Raman noise source due to the symmetrical spatial response, the spatial covariances of eq. (6.4) can be written as:

$$S^{(n)}(x,x') = \Phi_{NL}^2 \int ds g(x-s)\, g(x'-s)\, e_{IN}^2(s)\, e_{IN}(x)\, e_{IN}(x') \tag{6.12}$$

$$S^{(n)}(x,x') = \left\{ \begin{array}{c} i\Phi_{NL} g(x'-x)\, e_{IN}(x)\, e_{IN}(x') \\ -\Phi_{NL}^2 \int ds g(x-s)\, g(x'-s)\, e_{IN}^2(s)\, e_{IN}(x)\, e_{IN}(x') \end{array} \right\} \tag{6.13}$$

The kernel matrix assumes the form:

$$S(x,x') = \left[\begin{array}{c|c} 0 & \Phi_{NL} g(x'-x) \\ \hline \Phi_{NL} g(x'-x) & 2\Phi_{NL}^2 \int ds g(x-s)\, g(x'-s)\, e_{IN}^2(s) \end{array} \right] e_{IN}(x)\, e_{IN}(x') \tag{6.14}$$

6.3.1 The iterated kernel method of solution

If we let:

$$K_B(x,x') = g(x'-x)\, e_{IN}(x)\, e_{IN}(x') \tag{6.15}$$

and:

$$\begin{aligned} K_B^{(2)}(x,x') &= \int ds K_B(x,s)\, K_B(s,x') \\ &= \int ds g(x-s)\, g(x'-s)\, e_{IN}^2(s)\, e_{IN}(x)\, e_{IN}(x') \end{aligned} \tag{6.16}$$

as the iterated kernel of $K_B(x,x')$, then eq. (6.14) can be succinctly put in the following

form:

$$S(x,x') = \left[\begin{array}{c|c} 0 & \Phi_{NL}K_B(x,x') \\ \hline \Phi_{NL}K_B(x,x') & 2\Phi_{NL}^2 K_B^{(2)}(x,x') \end{array}\right] \tag{6.17}$$

Then, $K_B(x,x')$ is symmetric with an orthonormal set of eigenfunctions, which can be made complete by Gram-Schmidt orthogonalization if we include the null-space:

$$K_B(x,x') = \sum_{i=0}^{\infty} \lambda_{Bi}\Phi_{Bi}(x)\,\Phi_{Bi}(x') \tag{6.18}$$

$$\int dx \Phi_{Bi}(x)^T \Phi_{Bj}(x) = \delta_{ij} \tag{6.19}$$

and:

$$K_B^{(2)}(x) = \sum_{i=0}^{\infty} \lambda_{Bi}^2 \Phi_{Bi}(x)\,\Phi_{Bi}(x') \tag{6.20}$$

Since $\Phi_{Bi}(x)$ are eigenfunctions of each term of the kernel matrix (6.14), we guess a function normalized in the sense of eq. (6.10):

$$\gamma_i(x) = \begin{bmatrix} \Phi_{Bi}(x)\cos\phi \\ \Phi_{Bi}(x)\sin\phi \end{bmatrix} \tag{6.21}$$

and substitute it in the integral of eq. (6.9). It is found to satisfy:

$$\int dv S(x,x')\,\gamma_i(x') = \begin{bmatrix} \Phi_{NL}\lambda_{Bi}\sin\phi \\ \Phi_{NL}\lambda_{Bi}\cos\phi + 2\Phi_{NL}^2\lambda_{Bi}^2\sin\phi \end{bmatrix} \Phi_{Bi}(x) \tag{6.22}$$

If we can find a ϕ such that

$$\begin{bmatrix} \Phi_{NL}\lambda_{Bi}\sin\phi \\ \Phi_{NL}\lambda_{Bi}\cos\phi + 2\Phi_{NL}^2\lambda_{Bi}^2\sin\phi \end{bmatrix} = \lambda_i \begin{bmatrix} \cos\phi \\ \sin\phi \end{bmatrix} \tag{6.23}$$

for some λ_i, then $\gamma_i(x)$ will exactly satisfy the integral equation (6.9). Eq. (6.23) can be solved for non-zero λ_{Bi} to give:

$$\tan(2\phi) = -\frac{1}{\lambda_{Bi}\Phi_{NL}} \tag{6.24}$$

which has two solutions for ϕ, differing by $\frac{\pi}{2}$, each with a distinct eigenvalue:

$$\begin{aligned} \lambda_i &= \pm\frac{\lambda_{Bi}\Phi_{NL}}{\sqrt{1+\lambda_{Bi}^2\Phi_{NL}^2}} + \lambda_{Bi}^2\Phi_{NL}^2\left[1 \pm \frac{\lambda_{Bi}\Phi_{NL}}{\sqrt{1+\lambda_{Bi}^2\Phi_{NL}^2}}\right] \\ &= \lambda_{Bi}^2\Phi_{NL}^2 \pm \lambda_{Bi}\Phi_{NL}\sqrt{1+\lambda_{Bi}^2\Phi_{NL}^2} \end{aligned} \tag{6.25}$$

and an eigenvector:

$$\gamma_i(x) = \begin{bmatrix} -\frac{1}{\sqrt{2}}\left(1 \pm \frac{\lambda_{Bi}\Phi_{NL}}{\sqrt{1+\lambda_{Bi}^2\Phi_{NL}^2}}\right)^{1/2}\Phi_{Bi}(x) \\ \pm\frac{1}{\sqrt{2}}\left(1 \mp \frac{\lambda_{Bi}\Phi_{NL}}{\sqrt{1+\lambda_{Bi}^2\Phi_{NL}^2}}\right)^{1/2}\Phi_{Bi}(x) \end{bmatrix} \tag{6.26}$$

In eq. (6.25) and (6.26) the signs are assumed paired, and belong to the two values of ϕ that satisfy eq. (6.24). Hence a phase-shift of $\frac{\pi}{2}$ yields another eigenfunction of the kernel $S(x, x')$. We can substitute the minimum of the eigenvalues from eq. (6.25) in eq. (6.11) to get the minimum noise spectrum corresponding to the eigenfunction $\gamma_i(x)$:

$$S_N = \left[\sqrt{1+\lambda_{Bi}^2\Phi_{NL}^2} - \lambda_{Bi}\Phi_{NL}\right]^2 \tag{6.27}$$

which is essentially the Bogoliubov transformation result of chapter 1, and decreases with $\lambda_{Bi}\Phi_{NL}$. At any Φ_{NL}, the minimum noise therefore occurs for the highest λ_{Bi}.

6.4 Exact solution of the optimization problem for a Gaussian spatial excitation and a Gaussian spatial response

Next, we choose the exact form of the spatial response and the pump profile. Both of these are assumed to be Gaussian, with different decay lengths over the width of the fiber:

$$g(x) = \frac{1}{\sqrt{\pi}L_g}\exp\left(-\frac{x^2}{L_g^2}\right) \tag{6.28}$$

$$e_{IN}(x) = \exp\left(-\frac{x^2}{L_{IN}^2}\right) \tag{6.29}$$

Eq. (6.15) for $K_B(x, x')$ is expressible as:

$$K_B(x, x') = \frac{1}{\sqrt{\pi}L_g}\exp\left(-\frac{(x'-x)^2}{L_g^2}\right)\exp\left(-\frac{x^2}{L_{IN}^2}\right)\exp\left(-\frac{x'^2}{L_{IN}^2}\right) \tag{6.30}$$

which is a positive definite, symmetric function, and therefore possesses a complete, orthonormal set of eigenfunctions.

If we could solve for the eigenfunctions and eigenvalues of $K_B(x, x')$, the eigenfunctions and eigenvalues of $S(x, x')$ would simply follow from eqs. (6.25) and (6.26). Indeed, we have the exact eigenvalues and eigenfunctions of $K_B(x, x')$, and these are the Hermite-Gaussian modes:

$$\Phi_{Bi}(x) = C_i e^{-\left(d\sqrt{(d^2+2)}\frac{x^2}{L_g^2}\right)} H_i\left(\frac{\sqrt{2d\sqrt{(d^2+2)}}\,x}{L_g}\right) \qquad i = 0, 1, 2, \text{----} \tag{6.31}$$

where $d = \frac{L_g}{L_{IN}}$ and C_i is the normalization constant for the mode, given by:

$$C_i = \left[\frac{\sqrt{2d\sqrt{(d^2+2)}}}{i!2^i\sqrt{\pi}L_g}\right]^{1/2} \tag{6.32}$$

The function $H_i(x)$ is the Hermite mode of order i. The eigenvalues λ_{Bi} associated with

each eigenfunction $\Phi_{Bi}(x)$ are:

$$\lambda_{Bi} = \frac{\left(1 + d^2 - d\sqrt{(d^2+2)}\right)^{i/2}}{\left(1 + d^2 + d\sqrt{(d^2+2)}\right)^{\frac{i+1}{2}}} \qquad i = 0, 1, 2, \text{------} \tag{6.33}$$

Proof:

From ref. [29], formula 7.374.8:

$$\int dx e^{-(x-y)^2} H_i(\alpha x) = \sqrt{\pi}\,[1-\alpha^2]^{i/2} H_i\left(\frac{\alpha y}{\sqrt{1-\alpha^2}}\right) \tag{6.34}$$

and formula 7.374.1:

$$\int dx e^{-x^2} H_n(x) H_m(x) = \delta_{nm} 2^n n! \sqrt{\pi} \tag{6.35}$$

the proof follows after a few changes of variables.

Let $u = \frac{x}{L_g}$, $w = \frac{x'}{L_g}$ and $d = \frac{L_g}{L_{IN}}$, then from eqs. (6.15), (6.28), and (6.29):

$$\begin{aligned}\int dx' K_B(x,x')\,\Phi_{Bi}(x') &= \frac{1}{\sqrt{\pi}L_g}\int dx' \exp\left(-\frac{x^2}{L_{IN}^2}\right)\exp\left(-\frac{(x-x')^2}{L_g^2}\right)\exp\left(-\frac{x^2}{L_{IN}^2}\right)\Phi_{Bi}(x') \\ &= \frac{1}{\sqrt{\pi}}\int dw \exp(-d^2u^2)\exp(-(u-w)^2)\exp(-d^2w^2)\,\psi_{Bi}(w)\end{aligned} \tag{6.36}$$

where $\psi_{Bi}(w) = \Phi_{Bi}(wL_g)$.

We assume an eigenfunction that satisfies eq. (6.35) for orthogonality:

$$\psi_{Bi}(w) = C_i e^{-\frac{\alpha^2}{2}w^2} H_i(\alpha w) \tag{6.37}$$

Substituting eq. (6.37) in eq. (6.36), and employing a second change of variables to get eq. (6.36) in a form similar to eq. (6.34):

$$w' = w\sqrt{1 + d^2 + \frac{\alpha^2}{2}} \tag{6.38}$$

$$u' = \frac{u}{\sqrt{1 + d^2 + \frac{\alpha^2}{2}}} \tag{6.39}$$

we reduce eq. (6.36) to:

$$\int dx' K_B(x, x')\,\Phi_{Bi}(x') = \left\{ \begin{array}{c} \frac{1}{\sqrt{\pi}}\left(1 + d^2 + \frac{\alpha^2}{2}\right)^{-1/2} \mathrm{x} \\ \exp\left(-\left(1 - (1 + d^2)\left(1 + d^2 + \frac{\alpha^2}{2}\right)\right)u'^2\right)\mathrm{x} \\ \int dw' \exp\left(-(u' - w')^2\right) H_i\left(\frac{\alpha}{\sqrt{1 + d^2 + \frac{\alpha^2}{2}}} w'\right) \end{array} \right\} \tag{6.40}$$

which further simplifies due to eq. (6.34) to:

$$\begin{aligned} \int dx' K_B(x, x')\,\Phi_{Bi}(x') &= \left(1 + d^2 + \frac{\alpha^2}{2}\right)^{-1/2}\left[1 - \frac{\alpha^2}{1 + d^2 + \frac{\alpha^2}{2}}\right]^{i/2} \mathrm{x} \\ &\exp\left(-\left(1 - (1 + d^2)\left(1 + d^2 + \frac{\alpha^2}{2}\right)\right)u'^2\right) H_i\left(\frac{\alpha}{\sqrt{1 + d^2 - \frac{\alpha^2}{2}}} u'\right) \end{aligned} \tag{6.41}$$

We now substitute back eq. (6.39) for u' into eq. (6.41), and impose the condition that $\Phi_{Bi}(x)$ be an eigenfunction of $K_B(x, x')$. This implies:

$$\left(1 + d^2 - \frac{\alpha^2}{2}\right)\left(1 + d^2 + \frac{\alpha^2}{2}\right) = 1 \tag{6.42}$$

which yields:

$$\alpha = \sqrt{2d\sqrt{(d^2 + 2)}} \tag{6.43}$$

The normalization constant C_i of eq. (6.37) is easily obtainable from eq. (6.35), and the

eigenvalue λ_{Bi} from do (6.41) by using the value of α from eq. (6.43).

Finally, we check if we have all the eigenfunctions of $K_B(x, x')$ by examining its trace and seeing if it is the same as the sum of the eigenvalues λ_{Bi}.

$$\int dx K_B(x,x) = \frac{1}{\sqrt{\pi}L_g}\int dx \exp\left(-2\frac{x^2}{L_{IN}^2}\right) = \frac{1}{\sqrt{2}L_g}L_{IN} = \frac{1}{\sqrt{2}d} \tag{6.44}$$

Also:

$$\begin{aligned}\sum_{i=0}^{\infty}\lambda_{Bi} &= \frac{1}{\left(1+d^2+d\sqrt{(d^2+2)}\right)^{1/2}}\sum_{i=0}^{\infty}\left(\frac{1+d^2-d\sqrt{(d^2+2)}}{1+d^2+d\sqrt{(d^2+2)}}\right)^{i/2} \\ &= \frac{1}{\left(1+d^2+d\sqrt{(d^2+2)}\right)^{1/2}}\frac{1}{1-\left(\frac{1+d^2-d\sqrt{(d^2+2)}}{1+d^2+d\sqrt{(d^2+2)}}\right)^{1/2}} \\ &= \frac{1}{\left(1+d^2+d\sqrt{(d^2+2)}\right)^{1/2}-\left(1+d^2-d\sqrt{(d^2+2)}\right)^{1/2}}\end{aligned} \tag{6.45}$$

the denominator of the last term looks complicated, but admits to simplification:

$$\begin{aligned}&\left(1+d^2+d\sqrt{(d^2+2)}\right)^{1/2}-\left(1+d^2-d\sqrt{(d^2+2)}\right)^{1/2} \\ &= \sqrt{1+d^2+d\sqrt{(d^2+2)}+1+d^2-d\sqrt{(d^2+2)}-2\sqrt{(1+d^2)^2-d^2(d^2+2)}} \\ &= \sqrt{2}d\end{aligned} \tag{6.46}$$

and this verifies that we have all the eigenvalues and eigenfunctions of $K_B(x, x')$.

Since the minimum value of λ_i in eq. (6.25) corresponds to the maximum λ_{Bi}, and because eq. (6.33) tells us that λ_{Bi} are arranged in a decreasing order, we choose as the optimal local-oscillator $\gamma_0(x)$.

6.5 Discussion and comparison of specific cases

If we specialize to the case $L_g = L_{IN}$, we can be a bit more explicit about the optimal spectrum and compare it to the spectrum of the next best available mode. As $d = 1$ for this case, the first two eigenvalues are:

$$\lambda_{B0} = \frac{1}{\sqrt{2+\sqrt{3}}} = \sqrt{2-\sqrt{3}} \tag{6.47}$$

$$\lambda_{B1} = \frac{\sqrt{2-\sqrt{3}}}{2+\sqrt{3}} = (2-\sqrt{3})^{3/2} \tag{6.48}$$

The optimal squeezing at any Φ_{NL} is therefore:

$$S_N = \left[\sqrt{1+\lambda_{B0}^2\Phi_{NL}^2} - \lambda_{B0}\Phi_{NL}\right]^2 \tag{6.49}$$

which has a leading term of $\frac{1}{4\lambda_{B0}^2\Phi_{NL}^2}$ in its asymptotic expansion. Similarly the leading term for the next mode is $\frac{1}{4\lambda_{B1}^2\Phi_{NL}^2}$, and implies a squeezing loss of:

$$10.\log(\lambda_{B0}^2) - 10.\log(\lambda_{B1}^2) = 11.44 \text{ dB} \tag{6.50}$$

at high Φ_{NL} if we were to switch from using the lowest order Hermite-Gaussian mode, which is just a Gaussian profile, to the next spatial mode, which has a Gaussian envelope and a linear modulation:

$$\Phi_{B1}(x) = \sqrt{\frac{2}{\pi}}\left[\frac{\sqrt{2d\sqrt{(d^2+2)}}}{L_g}\right]^{3/2} xe^{-\left(d\sqrt{(d^2+2)}\frac{x^2}{L_g^2}\right)} \tag{6.51}$$

This corresponds to a differentiation of the Fourier transform ($\tilde{\Phi}_{B1}(k_x)$)of the Gaussian envelope in the spatial frequency (k_x) domain:

$$\tilde{\Phi}_{B1}(k_x) = i\left[\frac{2}{\pi}\frac{L_g}{\sqrt{2d\sqrt{(d^2+2)}}}\right]^{1/2} k_x e^{-\left(\frac{L_g k_x^2}{4d\sqrt{(d^2+2)}}\right)} \tag{6.52}$$

The resulting spatial Fourier transform has no frequency component at $k_x = 0$. On the contrary, a Gaussian spatial response (eq. (6.28)) has a Gaussian spatial Fourier transform:

$$G(k_x) = \int dx g(x) e^{ik_x x} = \exp\left(-\left(\frac{L_g}{2}k_x\right)^2\right) \tag{6.53}$$

which peaks at $k_x = 0$. Hence the Kerr-interaction is very weak between the pump and the spatial response for the second mode, and squeezing suffers significantly.

We can predict the effect of choosing varying input beam-widths by observing that λ_{B0} is a monotonically decreasing function of d. Hence spatially wider pump beams have a better chance at reducing noise than spatially confined beams. Physically, this makes sense because we expect that a spatially wider beam is more confined in the spatial frequency k_x. A wider pump beam therefore sees a stronger Kerr-interaction as its spatial frequency contents are predominantly at low frequencies, experiencing a higher degree of squeezing.

It is also worthwhile addressing the squeezing limitations that arise from the non-localized Gaussian spatial response vis-a-vis the assumed $g(\vec{r}) = \delta(\vec{r})$ spatial response of the earlier chapters. The CW operation for the spatially "instantaneous" response was seen to have a leading term of $\frac{1}{4\Phi_{NL}^2}$. With the condition $\lambda_{B0} \leq 1$ implicit in eq. (6.33), with equality if $d = 0$, there is invariably some loss of squeezing involved for a Gaussian response of eq. (6.28) over a response $g(\vec{r}) = \delta(\vec{r})$. It is given by:

$$-10.\log(\lambda_{B0}^2) \quad \text{dB} \tag{6.54}$$

which has a value of 5.72 dB for $L_g = L_{IN}$. In fact, it is obvious from eq. (6.49) that a finite width Gaussian response will afford lesser noise squeezing than a $g(\vec{r}) = \delta(\vec{r})$ response for which $S_N = \left[\sqrt{1 + \Phi^2_{NL}} - \Phi_{NL}\right]^2$.

As a closing remark for this chapter, we would like to add that the Gaussian response whose treatment was restricted to a single dimension here, is generalizable to two dimensions. We can always choose orthogonal axes such that the Gaussian response is separable in the two coordinates, and then a simple extension of the one-dimensional results derived in this chapter hold.

Over all, we have demonstrated that the optimization framework of chapter 2 is quite versatile in its application, the most general case we can imagine being that of a spatio-temporal kernel matrix generated by spatial and time-dependent correlations in the signal field. The local-oscillator would then be a function of both space and time, and we expect that in general, analytical results as the one presented above may be hard to find. As done in this chapter, the general framework of chapter 2 can be adapted in a straightforward manner and results parallel to those of chapter 2 apply.

Chapter 7

Conclusions

In this thesis we addressed the problem of local-oscillator optimization for maximum noise squeezing in balanced homodyne detection. We developed a criterion for measuring the signal generated noise in a homodyne detector, namely the variance of accumulated charge associated with the detector photo-current. Through the mixing of incoming signal with a strong coherent-state local-oscillator beam, we can select the component of the signal beam in phase with the local-oscillator, and detect it as a photo-current generated by the homodyne detector. Based on this fact, we devised a mathematical framework in which the search for a local-oscillator to minimize the charge-variance σ_N^2 (normalized by its shot-noise level) could be posed appropriately from a system-theoretic point of view, and then proceeded to show how a local-oscillator could be chosen to minimize the normalized charge-variance. In principle, we solved the problem by the eigenfunction-eigenvalue approach of chapter 2 through eq. (2.15). Given a general scheme for signal generation, the said formalism provides a rigorous framework to find the minimum achievable noise level and the local-oscillator that achieves that squeezing.

For a phase-sensitive detection scheme to reduce the detected noise below the shot-noise, or coherent-state signal noise level, the signal needs to be in a squeezed state. From among the traditional squeezed state generation methods, we chose to study fiber FWM. For this purpose, we first explored the instantaneous interaction and found that the optimal local-oscillator was a very narrow pulse timed at the peak of the pump pulse. We then specialized a model recently presented by Boivin, Kärtner, and Haus [23] to the FWM regime, and considered it at fiber lengths and peak pump powers at which FWM has been studied experimentally. The most notable facet of this model is the inclusion of a Raman noise source to preserve commutator brackets, which leads to the presence of an additive

noise at all frequencies and temperatures. Inherent in the model is the relation between the noise sources and the fiber response, which can be chosen freely as long as it meets causality, and the condition (3.6) on phase and absolute integrability. The simplest such model that matches some key parameters like the Kerr coefficient and $H_i'(0)$ is a two-pole impulse response, which we study extensively from then on.

A CW analysis of the fiber FWM ensued, in which we found that the noises at different frequencies were uncorrelated for a CW pump. The minimum noise spectrum in that case was found by tuning over the frequency of observation. Unsurprisingly, wherever the Raman noise ($H_i(\omega)$) was strong, or the Kerr-interaction ($H_r(\omega)$)was weak, the homodyne noise was higher. From the comparative analysis at absolute zero temperature and $\omega = 0$, and at non-zero temperatures and $\omega > 0$, we found that only the former escaped having a fixed non-zero bound on the σ_N^2 that could be attained at high Φ_{NL}. At the rest of the temperatures and frequencies, the asymptotic expansion (4.15) predicted that the spectrum would not go below a floor that depends on the specific frequency and temperature. We discovered further that different terms in the asymptotic expansion corresponded to the rate at which the floor is approached and they steer the noise behavior at lower nonlinear phase-shifts, Φ_{NL}.

Then we dedicated our efforts to seeking bounds of the same sort on the pulsed squeezing. Complications arose because of the mixing of noise frequencies in the pulsed case, and explicit optimal local-oscillators could not be solved for in closed form. Another strategy was needed, and we decided to look for strong lower bounds on the noise, which we surmised, could be used to search over a class of square integrable local-oscillators.

We realized that bounds at every Φ_{NL} would not be realistic, and instead chose to characterize the optimal local-oscillator in the high Φ_{NL} limit. One of the first results we produced was that if a local-oscillator were to keep the noise from going above the shot-noise level, its phase would have to be nearly constant at high Φ_{NL}. A series of results followed, the most important one being the asymptotic expansion of σ_N^2. Through this result,

which assumed a constant phase local-oscillator, we were able to establish a noise-floor on σ_N^2, and a condition (5.22) to remove that noise-floor. We demonstrated further that the noise-floor was not removable for an important class of fiber response models: causal responses having rational transfer functions. We made use of the phase and absolute integrability restrictions on the allowed fiber responses to state the latter result.

Interesting issues came up when we investigated certain pulsed pump shapes and local-oscillators for their squeezing performance with regards to the instantaneous and the two-pole response models. We tested two different pumps, the Gaussian pump and the single-sided exponential pump, and for each of them we computed the noise for three different chirp-compensated local-oscillators: bright-fringe, pulse-compressed, and the weak-signal FWM local-oscillator. Out of the three local-oscillators, the weak-signal FWM was the only one with a time-dependent phase on it (besides the chirp compensation).

We found that the bright-fringe and pulse-compressed local-oscillators always leveled out to noise-floors, whereas the weak-signal local-oscillator actually beat the noise-floor in the instantaneous case. The floor calculations for the instantaneous response matched well with the observed noise levels, and the reason we gave for the absence of noise-floor in the weak-signal FWM case was that its phase was able to keep pace with the growing Φ_{NL}^2 in the asymptotic expansion, thus exactly compensating its effect, a result we verified through its σ_N^2 expansion. Even the weak-signal FWM local-oscillator could not defeat the noise-floor when it came to the two-pole response, hinting to our earlier result that for this response a zero noise-floor was a virtual impossibility, as it conformed to the rational transfer function class of responses.

A stark difference between the Gaussian and single-sided exponential pump cases was the noise-floor behavior for the non-instantaneous response, pulse-compressed local-oscillators. The Gaussian case displayed a tendency to revert to the shot-noise level both for very broad and very narrow local-oscillators, and the approach to the noise-floor became rapid at both of these compressions. We were forced to conclude that none of these

extremes was desirable as an optimal local-oscillator, which would therefore have to lie between the two, at least at high Φ_{NL}. The single-sided exponential, however, due to its discontinuity at $t = 0$, functioned in a way that diminished the floor at high compressions. This was not sufficient justification for the single-sided exponential to be the optimal local-oscillator. The next term in the asymptotic expansion blew up at high local-oscillator compressions, prohibiting the optimal local-oscillator from being a highly compressed pulse.

Our final endeavor in this thesis was to seek a generalization of the time-dependent local-oscillator optimization to a general spatio-temporal optimization. Without going too far into the abstract details of the framework, which is a natural extension of the chapter 2 results, we headed straight for a particular case. We assumed a spatio-temporal FWM interaction with Gaussian spatial response in a single dimension, and an instantaneous temporal response. The spatial symmetry took away the need for noise sources to preserve commutator brackets. Then we assumed a CW pump with a one-dimensional Gaussian profile. As a consequence, the kernel matrix of eq. (2.15) assumed a very nice structure. We found a temporal Bogoliubov transformation with spatial variation in covariances, which led to a spatial eigenvalue-eigenfunction decomposition for optimal local-oscillator. The spatial modes turned out to be Gauss-Hermite functions and we could exactly determine the optimal noise behavior. We witnessed that a Gaussian spatial response, even with an optimal local-oscillator choice, came up short of the squeezing attainable in chapter 1 for the instantaneous response CW case. Also, there were significant advantages to be gained in squeezing, if the local-oscillator was appropriately mode-matched to the response, and fared much better than any other mode selection. The intent of chapter 6 was two-fold. The first to present a very striking and elegant solution to a spatial local-oscillator optimization, and the second to broaden the scope of our framework to include spatial ferritins in the signal covariances. We found it sufficient to state that the one-dimensional optimization can be easily extended to a two-dimensional spatial interaction

for the Gaussian response case, and the essentials were embodied in the analysis presented.

As regards the future work in this direction, we still have some unanswered questions which might bear looking into. The first has to do with the numerical solution to the eigenvalue-eigenfunction problem for the cases we studied. That would give us an estimate of how close the local-oscillators we tried came to being the optimal. It would also help develop the machinery to optimize the local-oscillator for arbitrary time-dependent signal statistics. Then there is the issue of analytical bounds on the performance. Although eqs. (5.16) through (5.19) give us the high Φ_{NL} bounds on squeezing as a function of the local-oscillator $\rho_{LO}(t)$ used, it would be far better if a tight bound on the noise-floor independent of the local-oscillator could be found. It would not only set a strong limit on how much squeezing can be expected from choosing local-oscillators, but also facilitate the choice of a $\rho_{LO}(t)$ which comes close to meeting such a bound by making the bound dependent on the pump and the fiber response alone.

We might also want to know if the high Φ_{NL} bound on noise *is* the best achievable for a fiber FWM. To extend the results from section 5.1 to a global result for a noise minimum, we need a stronger condition: the optimal charge variance should decrease with higher Φ_{NL}. If we could establish this, it could be stated that no choice of local-oscillator will bring the charge variance to 0 for the class of fiber responses with rational transfer functions. Prior to this work, limits on FWM squeezing did not exist, but we have succeeded in showing that such may be the case.

The groundwork for further studies on optimal homodyne detection is now firmly in place. It is now needed that future studies should utilize our FWM work as a point of reference and delve into the unexplored areas of squeezing and optimal performance for the non-instantaneous model. These could be geared to exploit the self-phase modulation (SPM), which we expect to be bounded in performance by the FWM approximation.

Hence optimal local-oscillators for FWM approximation serve as natural first guesses for the exact SPM squeezing.

References

[1] J.H. Shapiro, "Quantum Noise and Excess Noise in Optical Homodyne and Heterodyne Receivers,"IEEE Journal of Quantum Electronics, Vol. QE-21, 237 (1985)

[2] H. P. Yuen, and V. W. S. Chan, "Noise in homodyne and heterodyne detection," Optics Letters Vol. 8, 177 (1983)

[3] B. L. Schumaker, "Noise in homodyne detection," Optics Letters Vol. 9, 189 (1984)

[4] D. F. Walls, "Squeezed states of light," Nature Vol. 306, 141 (1983)

[5] M. D. Levenson, R. M. Shelby, M. D. Reid, D. F. Walls, and A. Aspect, "Generation and detection of squeezed states of light by nondegenerate four-wave mixing in an optical fiber,"Phys. Rev. A32, 1550 (1985)

[6] M. Shirasaki, and H. A. Haus, "Squeezing of pulses in a nonlinear interferometer," J. Opt. Soc. Am. B. Vol. 7, 30 (1990)

[7] K. Bergman, and H. A. Haus, "Squeezing in fibers with optical pulses," Optics Letters, 663 (1991)

[8] T. Hirano, and M. Matsuoka, "Broadband squeezing of light by pulse excitation," Optics Letters Vol. 15, 1153 (1990)

[9] R. E. Slusher, P. Grangier, A. LaPorta, B. Yurke, and M. J. Potasek, "Pulsed Squeezed Light," Physical Review Letters Vol. 59, Number 22, 2566 (1987)

[10] O. Aytür, and P. Kumar, "Squeezed-light generation with a mode locked Q-switched laser and detection by using a matched local-oscillator," Optics Letters Vol. 17, 529 (1992)

[11] P. Kumar, O. Aytür, and J. Huang,"Squeezed Light Generation with an Incoherent Pump," Physical Review Letters Vol. 64, Number 9, 1015 (1989)

[12] B. Yurke, P. Grangier, R. E. Slusher, and M. J. Potasek, "Generating and detecting short-duration pulses of squeezed light," Phys. Rev. A35, 3586 (1987)

[13] L. J. Joneckis, and J. H. Shapiro, "Enhanced Fiber Squeezing Via Local-Oscillator Pulse Compression", Proceedings of Nonlinear Optics '94, Waikoloa, HI (IEEE, New York, 1994) pp. 347-349

[14] M. Shirasaki, and H. A. Haus, "Squeezing of pulses in a nonlinear interferometer," J. Opt. Soc. Am. B. Vol. 7, 30 (1990)

[15] L. Boivin, F. X. Kärtner, and H. A. Haus, "Analytical Solution to the Quantum Field Theory of Self-Phase Modulation with a Finite Response Time," Phys. Rev. Lett. 73, 240 (1994)

[16] J. H. Shapiro, and L. Boivin, "Raman-Noise Limit on Squeezing in Continuous Wave Four-Wave Mixing," Opt. Lett. Vol. 20, No. 8, 925 (1995)

[17] J. H. Shapiro, and L. G. Joneckis, "Quantum propagation in a Kerr medium: lossless, dispersionless fiber," J. Opt. Soc. Am. B, 1102 (1993)

[18] P. D. Townsend, and R. Loudon, "Quantum-noise reduction at frequencies up to 0.5 GHz using pulsed parametric amplification," Phys. Rev. A45, 458 (1992)

[19] A. La Porta, and R. E. Slusher, "Squeezing limits at high parametric gains," Phys. Rev. A44, 2013 (1991)

[20] C. Kim, R. Li, and P. Kumar, "Deamplification response of a traveling-wave phase-sensitive optical parametric amplifier," Optics Letters Vol. 19, 132 (1994)

[21] C. D. Green, *Integral Equation Methods*, (Barnes & Noble Inc., NY 1969)

[22] D. G. Luenberger, *Optimization by Vector Space Methods,* (John Wiley & Sons, NY 1969)

[23] L. Boivin, F. X. Kärtner, and H. A. Haus, "Analytical Solution to the Quantum Field Theory of Self-Phase Modulation with a Finite Response Time," Phys. Rev. Lett. 73, 240 (1994)

[24] K. J. Blow, R. Loudon, and S. J. D. Phoenix, "Exact solution for quantum self-phase modulation," J. Opt. Soc. Am. B/Vol. 8, No. 8, 1750 (1991)

[25] H. A. Haus, *Nonlinear Optics: Chapter 11*, (Kluwer Academic Publishers, Netherlands 1992)

[26] R. Loudon, *The Quantum Theory of Light,* (Oxford University Press 1991)

[27] L. Ma'te', *Hilbert Space Methods in Science and Engineering*, (Adam Hilger, NY 1989) pg. 252

[28] private communication to J. H. Shapiro.

[29] I. S. Gadshteyn, and I. M. Ryzhik, *Table of Integrals, Series, Products*, (Academic Press, NY 1980)